14. Shafer RW, Kozal MJ, Winters MA, Iversen AK, Katzenstein DA, et al. (1994) Combination therapy with zidovudine and didanosine selects for drug-resistant human immunodeficiency virus type 1 strains with unique patterns of pol gene mutations. J Infect Dis 169: 722–729.
15. Shirasaka T, Kavlick MF, Ueno T, Gao WY, Kojima E, et al. (1995) Emergence of human immunodeficiency virus type 1 variants with resistance to multiple dideoxynucleosides in patients receiving therapy with dideoxynucleosides. Proc Natl Acad Sci U S A 92: 2398–2402.
16. Iversen AK, Shafer RW, Wehrly K, Winters MA, Mullins JI, et al. (1996) Multidrug-resistant human immunodeficiency virus type 1 strains resulting from combination antiretroviral therapy. J Virol 70: 1086–1090.
17. Maeda Y, Venzon DJ, Mitsuya H (1998) Altered drug sensitivity, fitness, and evolution of human immunodeficiency virus type 1 with pol gene mutations conferring multi-dideoxynucleoside resistance. J Infect Dis 177: 1207–1213.
18. Matsumi S, Kosalaraksa P, Tsang H, Kavlick MF, Harada S, et al. (2003) Pathways for the emergence of multi-dideoxynucleoside-resistant HIV-1 variants. AIDS 17: 1127–1137.
19. Kosalaraksa P, Kavlick MF, Maroun V, Le R, Mitsuya H (1999) Comparative fitness of multi-dideoxynucleoside-resistant human immunodeficiency virus type 1 (HIV-1) in an In vitro competitive HIV-1 replication assay. J Virol 73: 5356–5363.
20. Garcia Lerma J, Schinazi RF, Juodawlkis AS, Soriano V, Lin Y, et al. (1999) A rapid non-culture-based assay for clinical monitoring of phenotypic resistance of human immunodeficiency virus type 1 to lamivudine (3TC). Antimicrob Agents Chemother 43: 264–270.
21. Feng JY, Myrick F, Selmi B, Deval J, Canard B, et al. (2005) Effects of HIV Q151M-associated multi-drug resistance mutations on the activities of (-)-beta-D-1′,3′-dioxolan guanine. Antiviral Res 66: 153–158.
22. Miller MD, Margot NA, Hertogs K, Larder B, Miller V (2001) Antiviral activity of tenofovir (PMPA) against nucleoside-resistant clinical HIV samples. Nucleosides Nucleotides Nucleic Acids 20: 1025–1028.
23. Smith RA, Gottlieb GS, Anderson DJ, Pyrak CL, Preston BD (2008) Human immunodeficiency virus types 1 and 2 exhibit comparable sensitivities to Zidovudine and other nucleoside analog inhibitors in vitro. Antimicrob Agents Chemother 52: 329–332.
24. Ueno T, Shirasaka T, Mitsuya H (1995) Enzymatic characterization of human immunodeficiency virus type 1 reverse transcriptase resistant to multiple 2′,3′-dideoxynucleoside 5′-triphosphates. J Biol Chem 270: 23605–23611.
25. Deval J, Selmi B, Boretto J, Egloff MP, Guerreiro C, et al. (2002) The molecular mechanism of multidrug resistance by the Q151M human immunodeficiency virus type 1 reverse transcriptase and its suppression using alpha-boranophosphate nucleotide analogues. J Biol Chem 277: 42097–42104.
26. Huang H, Chopra R, Verdine GL, Harrison SC (1998) Structure of a covalently trapped catalytic complex of HIV-1 reverse transcriptase: implications for drug resistance. Science 282: 1669–1675.
27. Sarafianos SG, Das K, Hughes SH, Arnold E (2004) Taking aim at a moving target: designing drugs to inhibit drug-resistant HIV-1 reverse transcriptases. Curr Opin Struct Biol 14: 716–730.
28. Gu Z, Fletcher RS, Arts EJ, Wainberg MA, Parniak MA (1994) The K65R mutant reverse transcriptase of HIV-1 cross-resistant to 2′, 3′-dideoxycytidine, 2′,3′-dideoxy-3′-thiacytidine, and 2′,3′-dideoxyinosine shows reduced sensitivity to specific dideoxynucleoside triphosphate inhibitors in vitro. J Biol Chem 269: 28118–28122.
29. Winters MA, Shafer RW, Jellinger RA, Mamtora G, Gingeras T, et al. (1997) Human immunodeficiency virus type 1 reverse transcriptase genotype and drug susceptibility changes in infected individuals receiving dideoxyinosine monotherapy for 1 to 2 years. Antimicrob Agents Chemother 41: 757–762.
30. Harrigan PR, Stone C, Griffin P, Najera I, Bloor S, et al. (2000) Resistance profile of the human immunodeficiency virus type 1 reverse transcriptase inhibitor abacavir (1592U89) after monotherapy and combination therapy. CNA2001 Investigative Group. J Infect Dis 181: 912–920.
31. Margot NA, Isaacson E, McGowan I, Cheng AK, Schooley RT, et al. (2002) Genotypic and phenotypic analyses of HIV-1 in antiretroviral-experienced patients treated with tenofovir DF. AIDS 16: 1227–1235.
32. Sluis-Cremer N, Arion D, Kaushik N, Lim H, Parniak MA (2000) Mutational analysis of Lys65 of HIV-1 reverse transcriptase. Biochem J 348 Pt 1: 77–82.
33. Deval J, Navarro JM, Selmi B, Courcambeck J, Boretto J, et al. (2004) A loss of viral replicative capacity correlates with altered DNA polymerization kinetics by the human immunodeficiency virus reverse transcriptase bearing the K65R and L74V dideoxynucleoside resistance substitutions. J Biol Chem 279: 25489–25496.
34. Feng JY, Myrick FT, Margot NA, Mulamba GB, Rimsky L, et al. (2006) Virologic and enzymatic studies revealing the mechanism of K65R- and Q151M-associated HIV-1 drug resistance towards emtricitabine and lamivudine. Nucleosides Nucleotides Nucleic Acids 25: 89–107.
35. Das K, Bandwar RP, White KL, Feng JY, Sarafianos SG, et al. (2009) Structural basis for the role of the K65r mutation in HIV-1 reverse transcriptase polymerization, excision antagonism, and tenofovir resistance. J Biol Chem 284: 35092–35100.
36. McColl DJ, Miller MD (2003) The use of tenofovir disoproxil fumarate for the treatment of nucleoside-resistant HIV-1. J Antimicrob Chemother 51: 219–223.
37. Chappell BJ, Margot NA, Miller MD (2007) Long-term follow-up of patients taking tenofovir DF with low-level HIV-1 viremia and the K65R substitution in HIV-1 RT. AIDS 21: 761–763.
38. Hachiya A, Kodama EN, Sarafianos SG, Schuckmann MM, Sakagami Y, et al. (2008) Amino acid mutation N348I in the connection subdomain of human immunodeficiency virus type 1 reverse transcriptase confers multiclass resistance to nucleoside and nonnucleoside reverse transcriptase inhibitors. J Virol 82: 3261–3270.
39. Shimura K, Kodama E, Sakagami Y, Matsuzaki Y, Watanabe W, et al. (2008) Broad antiretroviral activity and resistance profile of the novel human immunodeficiency virus integrase inhibitor elvitegravir (JTK-303/GS-9137). J Virol 82: 764–774.
40. Hachiya A, Aizawa-Matsuoka S, Tanaka M, Takahashi Y, Ida S, et al. (2001) Rapid and simple phenotypic assay for drug susceptibility of human immunodeficiency virus type 1 using CCR5-expressing HeLa/CD4(+) cell clone 1-10 (MAGIC-5). Antimicrob Agents Chemother 45: 495–501.
41. Michailidis E, Marchand B, Kodama EN, Singh K, Matsuoka M, et al. (2009) Mechanism of inhibition of HIV-1 reverse transcriptase by 4′-Ethynyl-2-fluoro-2′-deoxyadenosine triphosphate, a translocation-defective reverse transcriptase inhibitor. J Biol Chem 284: 35681–35691.
42. Singh K, Srivastava A, Patel SS, Modak MJ (2007) Participation of the fingers subdomain of Escherichia coli DNA polymerase I in the strand displacement synthesis of DNA. J Biol Chem 282: 10594–10604.
43. Kati WM, Johnson KA, Jerva LF, Anderson KS (1992) Mechanism and fidelity of HIV reverse transcriptase. J Biol Chem 267: 25988–25997.
44. Schuckmann MM, Marchand B, Hachiya A, Kodama EN, Kirby KA, et al. The N348I mutation at the connection subdomain of HIV-1 reverse transcriptase decreases binding to nevirapine. J Biol Chem.
45. Tuske S, Sarafianos SG, Clark AD, Jr., Ding J, Naeger LK, et al. (2004) Structures of HIV-1 RT-DNA complexes before and after incorporation of the anti-AIDS drug tenofovir. Nat Struct Mol Biol 11: 469–474.
46. Ren J, Nichols CE, Chamberlain PP, Weaver KL, Short SA, et al. (2004) Crystal structures of HIV-1 reverse transcriptases mutated at codons 100, 106 and 108 and mechanisms of resistance to non-nucleoside inhibitors. J Mol Biol 336: 569–578.
47. Clark S, Calef C, J M (2006) Mutations in Retroviral Genes Associated with Drug Resistance. HIV Sequence Compendium 2005: 58–175.
48. Meyer PR, Matsuura SE, So AG, Scott WA (1998) Unblocking of chain-terminated primer by HIV-1 reverse transcriptase through a nucleotide-dependent mechanism. Proc Natl Acad Sci U S A 95: 13471–13476.
49. Rigourd M, Ehresmann C, Parniak MA, Ehresmann B, Marquet R (2002) Primer unblocking and rescue of DNA synthesis by azidothymidine (AZT)-resistant HIV-1 reverse transcriptase: comparison between initiation and elongation of reverse transcription and between (−) and (+) strand DNA synthesis. J Biol Chem 277: 18611–18618.
50. Frankel FA, Marchand B, Turner D, Gotte M, Wainberg MA (2005) Impaired rescue of chain-terminated DNA synthesis associated with the L74V mutation in human immunodeficiency virus type 1 reverse transcriptase. Antimicrob Agents Chemother 49: 2657–2664.
51. Winters B, Montaner J, Harrigan PR, Gazzard B, Pozniak A, et al. (2008) Determination of clinically relevant cutoffs for HIV-1 phenotypic resistance estimates through a combined analysis of clinical trial and cohort data. J Acquir Immune Defic Syndr 48: 26–34.
52. Van Houtte M, Picchio G, Van Der Borght K, Pattery T, Lecocq P, et al. (2009) A comparison of HIV-1 drug susceptibility as provided by conventional phenotyping and by a phenotype prediction tool based on viral genotype. J Med Virol 81: 1702–1709.
53. Delaugerre C, Flandre P, Marcelin AG, Descamps D, Tamalet C, et al. (2008) National survey of the prevalence and conditions of selection of HIV-1 reverse transcriptase K70E mutation. J Med Virol 80: 762–765.
54. Kagan RM, Lee TS, Ross L, Lloyd RM, Jr., Lewinski MA, et al. (2007) Molecular basis of antagonism between K70E and K65R tenofovir-associated mutations in HIV-1 reverse transcriptase. Antiviral Res 75: 210–218.
55. Sluis-Cremer N, Sheen CW, Zelina S, Torres PS, Parikh UM, et al. (2007) Molecular mechanism by which the K70E mutation in human immunodeficiency virus type 1 reverse transcriptase confers resistance to nucleoside reverse transcriptase inhibitors. Antimicrob Agents Chemother 51: 48–53.
56. Van Laethem K, Pannecouque C, Vandamme AM (2007) Mutations at 65 and 70 within the context of a Q151M cluster in human immunodeficiency virus type 1 reverse transcriptase impact the susceptibility to the different nucleoside reverse transcriptase inhibitors in distinct ways. Infect Genet Evol 7: 600–603.
57. Larder BA, Kemp SD (1989) Multiple mutations in HIV-1 reverse transcriptase confer high-level resistance to zidovudine (AZT). Science 246: 1155–1158.
58. Johnson VA, Brun-Vezinet F, Clotet B, Gunthard HF, Kuritzkes DR, et al. (2009) Update of the drug resistance mutations in HIV-1: December 2009. Top HIV Med 17: 138–145.
59. Frangeul A, Bussetta C, Deval J, Barral K, Alvarez K, et al. (2008) Gln151 of HIV-1 reverse transcriptase acts as a steric gate towards clinically relevant acyclic phosphonate nucleotide analogues. Antivir Ther 13: 115–124.
60. Garforth SJ, Kim TW, Parniak MA, Kool ET, Prasad VR (2007) Site-directed mutagenesis in the fingers subdomain of HIV-1 reverse transcriptase reveals a specific role for the beta3-beta4 hairpin loop in dNTP selection. J Mol Biol 365: 38–49.
61. Sarafianos SG, Pandey VN, Kaushik N, Modak MJ (1995) Glutamine 151 participates in the substrate dNTP binding function of HIV-1 reverse transcriptase. Biochemistry 34: 7207–7216.

62. Frangeul A, Barral K, Alvarez K, Canard B (2007) In vitro suppression of K65R reverse transcriptase-mediated tenofovir- and adefovir-5′-diphosphate resistance conferred by the boranophosphonate derivatives. Antimicrob Agents Chemother 51: 3162–3167.
63. Sarafianos SG, Pandey VN, Kaushik N, Modak MJ (1995) Site-directed mutagenesis of arginine 72 of HIV-1 reverse transcriptase. Catalytic role and inhibitor sensitivity. J Biol Chem 270: 19729–19735.
64. Tu X, Das K, Han Q, Bauman JD, Clark AD, Jr., et al. Structural basis of HIV-1 resistance to AZT by excision. Nat Struct Mol Biol 17: 1202–1209.

Cell. Mol. Biol. 57 (1): 39-
Published on January 31, 2011; DOI 10.1170/T900

THE SUGAR RING CONFORMATION OF 4'-ETHYNYL-2-FLUORO-2'-DEOXYADENOSINE AND ITS RECOGNITION BY THE POLYMERASE ACTIVE SITE OF HIV REVERSE TRANSCRIPTASE

K.A. KIRBY[1], K. SINGH[1], E. MICHAILIDIS[1], B. MARCHAND[1], E.N. KODAMA[2],
N. ASHIDA[3], H. MITSUYA[4], M.A. PARNIAK[5], AND S.G. SARAFIANOS[1]✉

1 Christopher S. Bond Life Sciences Center, Department of Molecular Microbiology & Immunology, University of Missouri School of Medicine, Columbia, MO 65211, USA
2 Division of Emerging Infectious Diseases. Tohoku University School of Medicine, Sendai 980-8575, Japan
3 Yamasa Corporation, Chiba 288-0056, Japan
4 Department of Hematology and Infectious Diseases, Kumamoto University, Kumamoto 860-8556, Japan & Experimental Retrovirology Section, HIV/AIDS Malignancy Branch, NIH, Bethesda, MD 20892, USA
5 Department of Molecular Genetics & Biochemistry University of Pittsburgh School of Medicine, Pittsburgh, PA 15261, USA

Abstract

4'-Ethynyl-2-fluoro-2'-deoxyadenosine (EFdA) is the most potent inhibitor of HIV reverse transcriptase (RT). We have recently named EFdA a Translocation Defective RT Inhibitor (TDRTI) because after its incorporation in the nucleic acid it blocks DNA polymerization, primarily by preventing translocation of RT on the template/primer that has EFdA at the 3'-primer end (T/P_{EFdA}). The sugar ring conformation of EFdA may also influence RT inhibition by a) affecting the binding of EFdA triphosphate (EFdATP) at the RT active site and/or b) by preventing proper positioning of the 3'-OH of EFdA in T/P_{EFdA} that is required for efficient DNA synthesis. Specifically, the North (C2'-exo/C3'-endo), but not the South (C2'-endo/C3'-exo) nucleotide sugar ring conformation is required for efficient binding at the primer-binding and polymerase active sites of RT. In this study we use nuclear magnetic resonance (NMR) spectroscopy experiments to determine the sugar ring conformation of EFdA. We find that unlike adenosine nucleosides unsubstituted at the 4'-position, the sugar ring of EFdA is primarily in the North conformation. This difference in sugar ring puckering likely contributes to the more efficient incorporation of EFdATP by RT than dATP. In addition, it suggests that the 3'-OH of EFdA in T/P_{EFdA} is not likely to prevent incorporation of additional nucleotides and thus it does not contribute to the mechanism of RT inhibition. This study provides the first insights into how structural attributes of EFdA affect its antiviral potency through interactions with its RT target.

Key words: EFdA, Translocation Defective Reverse Transcriptase Inhibitors, Sugar Ring Conformation, Reverse Transcriptase, HIV, Antivirals.

Article information's
Received on December 17, 2010
Accepted on January 5, 2011

Corresponding author
Stefan G. Sarafianos, Ph.D.
471d Christopher S. Bond Life Sciences Center,
1201 Rollins St., Columbia, MO 65211, USA
Fax: +1 (573) 884 - 9676
E-mail: sarafianoss@missouri.edu

Abbreviations: **dA** : 2'-Deoxyadenosine ; **dATP** : 2'-Deoxyadenosine triphosphate ; **EFdA** : 4'-Ethynyl-2-fluoro-2'-deoxyadenosine ; **EFdAMP** : 4'-Ethynyl-2-fluoro-2'-deoxyadenosine monophosphate ; **EFdATP** : 4'-Ethynyl-2-fluoro-2'-deoxyadenosine triphosphate; **NRTI** : Nucleoside reverse transcriptase inhibitor; **RT** : Reverse transcriptase; $\mathbf{T/P_{EFdA}}$: Template/Primer terminated 4'-ethynyl-2-fluoro-2'-deoxyadenosine; **TDRTI**: Translocation defective reverse transcriptase inhibitor.

INTRODUCTION

HIV-1 reverse transcriptase (RT) is the most targeted viral protein by approved anti-HIV drugs due to its critical role in replication of the virus (24, 14, 29, 5, 32, 8). These inhibitors, which are either nucleoside reverse transcriptase inhibitors (NRTIs) or non-nucleoside reverse transcriptase inhibitors (NNRTIs), interfere with the enzyme's ability to synthesize the viral DNA. In particular, NRTIs mimic the natural dNTP substrate of the enzyme and bind to the 3'-primer terminus in the polymerase active site. Once incorporated into the primer, the NRTI prevents further elongation of the DNA by acting as a chain terminator. All currently approved NRTIs lack a 3'-OH moiety, which has long been considered a requirement for inhibitors to be successful chain terminators. Although this lack of a 3'-OH group promotes effective chain termination, it imparts a negative effect on the potency of the NRTI, including a diminished binding affinity for the RT target and decreased ability to be activated by cellular kinases (12).

We reported previously that a group of NRTIs with 4'-substitutions and a 3'-OH are very effective at inhibiting both wild-type (WT) and multi-drug resistant strains of HIV (18). The most potent compound in this collection is 4'-ethynyl-2-fluoro-2'-deoxyadenosine (EFdA), an adenosine analog containing a 4'-ethynyl group on the deoxyribose ring and a 2-fluoro group on the adenine base (Figure 1). EFdA is able to inhibit both WT and multi-drug resistant strains of HIV several orders of magnitude more efficiently than all other currently approved NRTIs (22). Moreover, clinically-observed drug resistant HIV strains are sensitive (38, 21), and in some cases hypersensitive (17), to EFdA. Recently, we have shown that EFdA acts primarily as a chain terminator because it prevents translocation of RT on the EFdA-terminated primer after incorporation. Antiviral compounds demonstrating this novel mechanism of inhibition have been termed Translocation Defective Reverse Transcriptase Inhibitors (TDRTIs) (22).

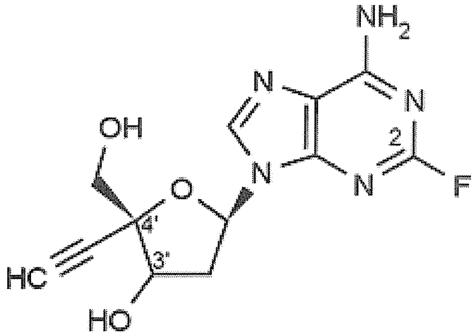

Figure 1. The chemical structure of EFdA.

It has been demonstrated that the conformation of the sugar ring affects the biological activity of NRTIs (16, 30, 27, 20, 25, 4, 31, 2, 3). In solution, the structure of the deoxyribose ring of nucleosides exists in a dynamic equilibrium between the C2'-exo/C3'-endo (North) and C2'-endo/C3'-exo (South) conformations. It has previously been shown that the sugar ring conformation of NRTIs is important for recognition by RT at both the primer and dNTP binding sites. For efficient DNA polymerization to occur, both the nucleotide at the 3'-end of the primer and the incoming dNTP or NRTI are required to be in the North conformation. In the North conformation, the 3'-OH of the nucleotide at the 3'-primer terminus is properly positioned for in-line nucleophilic attack on the α-phosphate of the incoming dNTP or NRTI (Figure 2a). The North conformation is also important for the incoming dNTP or NRTI, because if the sugar ring were in the South conformation, the 3'-OH would be very close to Tyr115 of RT (d = 1.8 Å), creating unfavorable steric interactions between the substrate and enzyme (Figure 2b) (20, 23, 2).

If EFdA were in the South conformation after incorporation into the primer, then the 3'-OH would not be properly positioned for in-line nucleophilic attack on the α-phosphate of the next incoming nucleotide, therefore contributing to inefficient catalysis and inhibition of DNA synthesis. In order to evaluate the influence of these structural attributes on the antiviral properties of EFdA, we carried out nuclear magnetic resonance (NMR) spectroscopy experiments using EFdA and the natural substrate dA. The results of this study allow us to compare the sugar ring puckering of EFdA and other nucleoside analogs, such as 2'-fluoro-2',3'-dideoxynucleoside 5'-triphosphates (23), AZT, ddI, ddA (26), and bicyclo[3.1.0]hexene nucleosides (28), and determine if its structure 1) is in the proper conformation for optimal recognition by RT and 2) if it contributes to the inhibition mechanism of HIV RT.

MATERIALS AND METHOD

Chemicals

The compound dA was purchased from Sigma-Aldrich (St. Louis, MO). EFdA was provided by Yamasa Corporation (Chiba, Japan). d_6-Dimethyl sulfoxide (DMSO) was purchased from Cambridge Isotope Laboratories, Inc. (Andover, MA). All other materials were purchased from Fisher Scientific (Pittsburgh, PA).

NMR Spectroscopy

One-dimensional ^{1}H NMR spectra were collected in 10 °C increments from 20 to 50 °C on a Bruker Avance DRX500 Spectrometer equipped with a 5mm HCN cryoprobe. Both dA and EFdA were dissolved in d_6-DMSO to final concentrations of 2 – 4 mM. Spectra used for coupling constant analysis were acquired with 64 scans and 33K data points with a sweep width of 4960 Hz and a relaxation delay of 4.3 s. Spectra were processed with a line broadening of 0.3 Hz. Coupling constants were read directly from the spectra for first-order resonances. Complex multiplets were analyzed by spectral simulation using SpinWorks 3.0 (19). Simulations were performed for the spin systems on the deoxyribose ring only. RMS deviations of calculated and experimental coupling constants for both compounds were < 0.05 Hz.

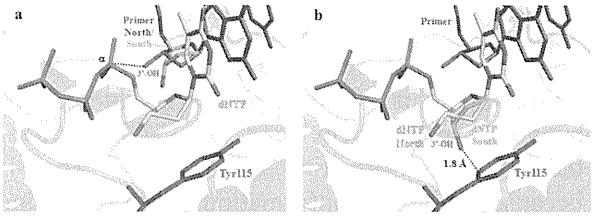

Figure 2. The effect of sugar ring conformation in the HIV-1 RT polymerase active site. The sugar ring conformation at the 3'-primer end is required to be in the North (2'-exo/3'-endo) conformation (2a, dark gray) for successful in-line nucleophilic attack of the α-phosphate of the incoming dNTP or NRTI. The South (2'-endo/3'-exo) (2a, green) conformation of the sugar ring at the primer terminus positions the 3'-OH away from the α-phosphate and thus DNA polymerization is not as efficient. The preferred conformation of the sugar ring of the incoming dNTP or NRTI is the North conformation (2b, yellow). The South conformation of the sugar ring of the incoming dNTP or NRTI (2b, green) would result in a very short distance between the 3'-OH and the aromatic ring of Tyr115 (red), causing steric interactions with the enzyme. Coot (10) was used to perform simple modeling of the 2'-endo/3'-exo sugar ring conformations of the primer and dNTP using structural coordinates from PDB Code 1RTD. Images were generated using PyMOL (7).

Pseudorotational Analysis

Sugar ring conformations of dA and EFdA were determined using the program PSEUROT 6.3 (13, 6, 36) (acquired from Dr. Cornelis Altona, University of Leiden, Netherlands). This version utilizes an improved generalized Karplus equation, as described by Donders et al. (9), which uses experimental data as a basis for the iterative calculation of coupling constants. In the case of dA, the puckering amplitude of the less favored conformation (ϕ_m(N)) was held constant during calculations. For EFdA, the puckering amplitudes of both conformations were fixed during calculation. RMS deviations of calculated and experimental coupling constants for both compounds were < 0.2 Hz.

Molecular Modeling

A model of the ternary complex of HIV-1 RT / DNA / EFdA triphosphate (EFdATP) was built using the coordinates of the crystal structure of the HIV-1 RT-DNA-tenofovir diphosphate (TFVDP) complex (35). The triphosphate of the EFdATP was built using the corresponding atoms of TFVDP in the structure from PDB code 1T05 and of dTTP in PDB code 1RTD (15). The structure of the EFdATP was assembled from its components using the sketch module of SYBYL 7.3 (34), and minimized by the semi-empirical quantum chemical method PM3 (33). After removing the TFVDP from 1T05, the PM3 charges and the docking module of SYBYL 7.0 were used to dock the EFdATP at the RT dNTP binding site to give the ternary complex of HIV-1 RT / DNA / EFdATP. The final complex structure was minimized for 100 cycles using the AMBER force field with Coleman united charges on the protein and DNA molecules.

RESULTS

NMR Spectroscopy and Pseudorotational Analysis

To evaluate the sugar ring conformation of dA and EFdA, one-dimensional ^{1}H NMR spectra were collected over a range of temperatures for both compounds. Coupling constants determined from each spectrum were used to calculate the structural parameters of the deoxyribose ring. The changes in the value of each coupling constant with temperature were examined for both compounds, and these changes were used to calculate the pseudorotational phase angle, P, and the degree of maximum ring pucker, ϕ_m, using PSEUROT 6.3 (Table 1) (1).

Coupling constants between most of the hydrogen atoms on the deoxyribose ring required spectral simulation in order to be resolved. The pseudorotational parameters listed in Table 1 were calculated with PSEUROT 6.3, which assumes a two-state approximation (North and South) and utilizes a generalized Karplus equation combined with a non-linear Newton-Raphson minimization process to examine the conformational flexibility of five-membered rings. An iterative approach was used to determine the optimal pseudorotational parameters P_N, P_S, ϕ_m(N), and ϕ_m(S) in which some of these parameters were fixed during refinement.

The results of the conformational analysis of dA demonstrate that the sugar ring heavily favors the South conformation over the North conformation in solution. This result is in agreement with previous conformational studies of dA (37, 11). On the other hand, the results of the conformational analysis of EFdA show that the sugar ring favors the North conformation in solution (Figure 3). The value of P_N is 38.7°, which is just slightly outside of the range observed for most typical nucleosides (P_N = 0 – 36°) but still in the Northern hemisphere (1). This observation is similar to that previously reported for 4'-ethynyl-2',3'-dideoxycytidine (31). The value of P_S is 146.5°, which falls in the range commonly observed for traditional nucleosides (P_S = 144 – 180°). The values of

Table 1. Summary of pseudorotational analysis. [a]Root mean square deviation between experimental and calculated coupling constants. [b]Parameter fixed during calculations.

Compound	P_N, deg	P_S, deg	$\phi_m(N)$, deg	$\phi_m(S)$, deg	% N	RMS error (Hz)[a]
dA	18.7	169.1	39.0[b]	31.1	23	0.034
EFdA	38.7	146.5	39.0[b]	39.0[b]	75	0.197

$\phi_m(N)$ and $\phi_m(S)$ were fixed during calculations to 39°, the average value commonly observed for purine-base nucleosides (1). This result suggests that either the 4'-ethynyl, 2-fluoro, or both in combination greatly influence the sugar ring conformation of EFdA compared to the natural substrate, dA.

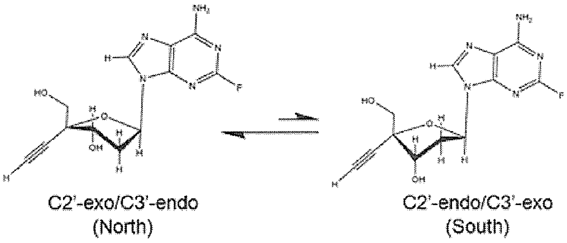

Figure 3. Dynamic equilibrium between the North and South sugar ring conformations of EFdA in solution.

To understand the molecular basis of importance of the sugar ring conformation for RT recognition, we used our pre-catalytic RT / DNA / EFdATP ternary complex to assess the effect of EFdA sugar ring conformation on the binding interactions of the inhibitor with the polymerase active site of the enzyme (Figure 4). In our molecular model, the 4'-ethynyl group is stabilized in a hydrophobic pocket formed by RT residues Ala114, Tyr115, Phe160, Met184, and the aliphatic segment of Asp185. With the 3'-carbon in the North conformation, the 3'-OH is able to fit nicely in the RT polymerase active site. However, when the 3'-carbon of EFdATP is placed in the South conformation, the 3'-OH interacts sterically with the aromatic ring of Tyr115 (short distance of 1.8 Å).

DISCUSSION

Our results show that EFdA has a dramatically different sugar ring conformation than dA. The equilibrium between the North and South sugar ring conformations is shifted from the preferred South conformation for the natural substrate dA to the North conformation for EFdA. It is not clear if the structural changes are due to the 2- or 4'-substitutions in EFdA. However, it is likely that steric interactions between the 4'-ethynyl and the 3'-OH disfavor the South conformation of EFdA. This is because the North conformation of the sugar ring positions the 4'-ethynyl and the 3'-OH groups farther apart than they would be in the South conformation. However, even in the absence of the 3'-OH, the sugar ring in the crystal structure of 4'-ethynyl-2',3'-dideoxycytidine is also in the North conformation (31). Hence, it appears that in addition to steric interactions between the 3'-OH and 4'-ethynyl, other factors contribute to the propensity of 4'-ethynyl-substituted NRTIs to have a sugar ring in the North conformation.

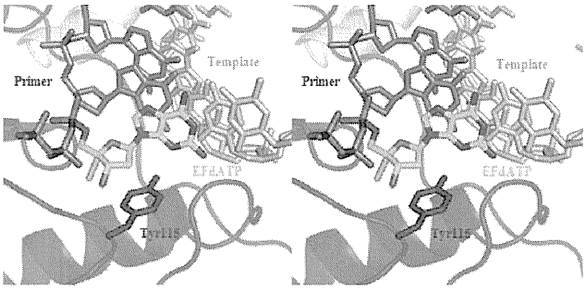

Figure 4. Stereo view of EFdATP (cyan) modeled in the RT active site. The 3'-OH of EFdATP is in the North conformation and is free of steric interactions with Tyr115 (red sticks). The primer is in dark gray, the template in light gray, the connection subdomain in yellow, and the palm subdomain in red. The fingers subdomain was removed for clarity. Image generated using PyMOL (7).

The NMR experiments confirm that EFdA is primarily in the North conformation, rendering its structure (and presumably the structure of its active metabolite EFdATP) in the optimal conformation for binding at the polymerase active site of RT. While the natural substrate, dA, favors the South conformation, the energy barrier required to convert the sugar ring of dA to the North conformation is very small, approximately 1 kcal/mol (11). EFdA (and presumably EFdATP) already favors the North conformation and does not have to overcome this energy barrier in order to bind to the primer. This is likely a contributing factor in the more efficient incorporation of EFdATP into the primer strand than dATP, contributing to the high potency of the inhibitor as reported (22).

Molecular modeling studies were performed with EFdATP to gain further insight into the structural effects of the sugar ring conformation on RT recognition. When EFdATP is positioned in the nucleotide binding site prior to incorporation into the primer, the importance of the sugar ring puckering becomes apparent. With the sugar ring of EFdATP positioned in the North conformation, the 3'-OH is free of unfavorable interactions with RT (particularly from steric interactions with Tyr115) and fits perfectly in the active site. In addition, the sugar ring geometry of EFdA allows favorable interactions of the 4'-ethynyl into a hydrophobic pocket defined by RT residues A114, Y115, F160, M184 and the aliphatic chain of D185. These interactions are thought to contribute both to enhanced RT utilization of EFdATP and difficulty in translocation of 3'-terminal EFdAMP primers (22).

Upon incorporation into the primer strand, the position of the 3'-OH of the EFdAMP in the North conformation is in perfect alignment for in-line nucleophilic attack on the α-phosphate of the next incoming dNTP. Because the North conformation of the sugar ring is heavily favored over the South conformation for EFdA, this is evidence that misalignment of the 3'-OH for nucleophilic attack is not a contributing factor to the chain termination mechanism of inhibition of EFdA. While the sugar ring conformation of the 3'-terminal EFdAMP is in the North conformation, which favors incorporation of the next dNTP, this step cannot occur because of the inability of RT to translocate from the nucleotide binding site. This further supports the observation that the inability of RT to translocate after EFdA incorporation is the primary mechanism of inhibition (22).

Slight changes in the chemical composition of adenosine analogs have a pronounced effect on the efficiency of TDRTIs in blocking HIV replication. In particular, substitutions at the 4'-position of the deoxyribose ring and the 2-position of the adenine base favor structural conformations of EFdA that improve its interactions with the RT target, thereby enhancing its antiviral potency.

Acknowledgements – We would like to thank Dr. Wei Wycoff for assistance with variable temperature NMR data collection. The purchase of the 500 MHz NMR spectrometer was partially supported by NSF grant CHE-89-08304, and NIH/NCRR grant S10 RR022341-01 (cold probe). This work was supported in part by NIH grants AI074389, AI076119, AI076119-S1, AI076119-02S1, and AI094715 (to S.G.S.) and AI079801 (to M.A.P.). We also acknowledge support from GeneMatrix and the Korea Food & Drug Administration and the Ministry of Knowledge and Economy, Bilateral International Collaborative R&D Program. B.M. is a recipient of the amfAR Mathilde Krim Fellowship. We are grateful to Yamasa Corporation for providing EFdA.

REFERENCES

1. Altona, C. and Sundaralingam, M., Conformational analysis of the sugar ring in nucleosides and nucleotides: A new description using the concept of pseudorotation. *J. Am. Chem. Soc.* 1972, **94**: 8205-8212.
2. Boyer, P.L., Julias, J.G., Marquez, V.E. and Hughes, S.H., Fixed conformation nucleoside analogs effectively inhibit excision-proficient HIV-1 reverse transcriptases. *J. Mol. Biol.* 2005, **345**: 441-450.
3. Boyer, P.L., Julias, J.G., Ambrose, Z., Siddiqui, M.A., Marquez, V.E. and Hughes, S.H., The nucleoside analogs 4'C-methyl thymidine and 4'C-ethyl thymidine block DNA synthesis by wild-type HIV-1 RT and excision proficient NRTI resistant RT variants. *J. Mol. Biol.* 2007, **371**: 873-882.
4. Choi, Y., George, C., Comin, M.J., Barchi, J.J., Jr., Kim, H.S., Jacobson, K.A., Balzarini, J., Mitsuya, H., Boyer, P.L., Hughes, S.H. and Marquez, V.E., A conformationally locked analogue of the anti-HIV agent stavudine. An important correlation between pseudorotation and maximum amplitude. *J. Med. Chem.* 2003, **46**: 3292-3299.
5. De Clercq, E., Anti-HIV drugs. *Verh. K. Acad. Geneeskd. Belg.* 2007, **69**: 81-104.
6. De Leeuw, F.A.A.M. and Altona, C., Computer assisted pseudorotational analysis of 5-membered rings by means of $^3J_{HH}$ coupling constants: program PSEUROT. *J. Comp. Chem.* 1983, **4**: 428-437.
7. DeLano, W.L. *The PyMOL Molecular Graphics System*, DeLano Scientific: Palo Alto, CA, USA, 2002. http://www.pymol.org.
8. Deval, J., Antimicrobial strategies: inhibition of viral polymerases by 3'-hydroxyl nucleosides. *Drugs* 2009, **69**: 151-166.
9. Donders, L.A., De Leeuw, F.A.A.M. and Altona, C., Relationship between proton-proton NMR coupling constants and substituent electronegativities. IV. An extended Karplus equation accounting for interactions between subtituents and its application to coupling constant data calculated by the extended Hueckel method. *Magn. Reson. Chem.* 1989, **27**: 556-563.
10. Emsley, P. and Cowtan, K., Coot: model-building tools for molecular graphics. *Acta Crystallogr. D Biol. Crystallogr.* 2004, **60**: 2126-2132.
11. Ford, H., Jr., Dai, F., Mu, L., Siddiqui, M.A., Nicklaus, M.C., Anderson, L., Marquez, V.E. and Barchi, J.J., Jr., Adenosine deaminase prefers a distinct sugar ring conformation for binding and catalysis: kinetic and structural studies. *Biochemistry.* 2000, **39**: 2581-2592.
12. Gallois-Montbrun, S., Schneider, B., Chen, Y., Giacomoni-Fernandes, V., Mulard, L., Morera, S., Janin, J.,

Deville-Bonne, D. and Veron, M., Improving nucleoside diphosphate kinase for antiviral nucleotide analogs activation. *J. Biol. Chem.* 2002, **277**: 39953-39959.
13. Haasnoot, C.A.G., De Leeuw, F.A.A.M., De Leeuw, H.P.M. and Altona, C., The relationship between proton-proton NMR coupling constants and substituent electronegativities II-Conformational analysis of the sugar ring in nucleosides and nucleotides in solution using a generalized Karplus equation. *Org. Magn. Reson.* 1981, **15**: 43-52.
14. Hammer, S.M., Saag, M.S., Schechter, M., Montaner, J.S., Schooley, R.T., Jacobsen, D.M., Thompson, M.A., Carpenter, C.C., Fischl, M.A., Gazzard, B.G., Gatell, J.M., Hirsch, M.S., Katzenstein, D.A., Richman, D.D., Vella, S., Yeni, P.G. and Volberding, P.A., Treatment for adult HIV infection: 2006 recommendations of the International AIDS Society--USA panel. *Top HIV Med.* 2006, **14**: 827-843.
15. Huang, H., Chopra, R., Verdine, G.L. and Harrison, S.C., Structure of a covalently trapped catalytic complex of HIV-1 reverse transcriptase: implications for drug resistance. *Science* 1998, **282**: 1669-1675.
16. Jagannadh, B., Reddy, D.V. and Kunwar, A.C., 1H NMR study of the sugar pucker of 2',3'-dideoxynucleosides with anti-human immunodeficiency virus (HIV) activity. *Biochem. Biophys. Res. Commun.* 1991, **179**: 386-391.
17. Kawamoto, A., Kodama, E., Sarafianos, S.G., Sakagami, Y., Kohgo, S., Kitano, K., Ashida, N., Iwai, Y., Hayakawa, H., Nakata, H., Mitsuya, H., Arnold, E. and Matsuoka, M., 2'-deoxy-4'-C-ethynyl-2-halo-adenosines active against drug-resistant human immunodeficiency virus type 1 variants. *Int. J. Biochem. Cell Biol.* 2008, **40**: 2410-2420.
18. Kodama, E.I., Kohgo, S., Kitano, K., Machida, H., Gatanaga, H., Shigeta, S., Matsuoka, M., Ohrui, H. and Mitsuya, H., 4'-Ethynyl nucleoside analogs: potent inhibitors of multidrug-resistant human immunodeficiency virus variants in vitro. *Antimicrob. Agents Chemother.* 2001, **45**: 1539-1546.
19. Marat, K. SpinWorks 3.0, released April 11, 2008. University of Manitoba, Winnipeg, Manitoba, Canada. http://www.umanitoba.ca/chemistry/nmr/spinworks/index.html.
20. Marquez, V.E., Ezzitouni, A., Russ, P., Siddiqui, M.A., Ford, H., Jr., Feldman, R.J., Mitsuya, H., George, C. and Barchi, J.J., Jr., HIV-1 Reverse Transcriptase Can Discriminate Between Two Conformationally Locked Carbocyclic AZT Triphosphate Analogues. *J. Am. Chem. Soc.* 1998, **120**: 2780-2789.
21. Mascolini, M., Larder, B.A., Boucher, C.A., Richman, D.D. and Mellors, J.W., Broad advances in understanding HIV resistance to antiretrovirals: report on the XVII International HIV Drug Resistance Workshop. *Antivir. Ther.* 2008, **13**: 1097-1113.
22. Michailidis, E., Marchand, B., Kodama, E.N., Singh, K., Matsuoka, M., Kirby, K.A., Ryan, E.M., Sawani, A.M., Nagy, E., Ashida, N., Mitsuya, H., Parniak, M.A. and Sarafianos, S.G., Mechanism of inhibition of HIV-1 reverse transcriptase by 4'-ethynyl-2-fluoro-2'-deoxyadenosine triphosphate, a translocation defective reverse transcriptase inhibitor. *J. Biol. Chem.* 2009, **284**: 35681-35691.
23. Mu, L., Sarafianos, S.G., Nicklaus, M.C., Russ, P., Siddiqui, M.A., Ford, H., Jr., Mitsuya, H., Le, R., Kodama, E., Meier, C., Knispel, T., Anderson, L., Barchi, J.J., Jr. and Marquez, V.E., Interactions of conformationally biased north and south 2'-fluoro-2', 3'-dideoxynucleoside 5'-triphosphates with the active site of HIV-1 reverse transcriptase. *Biochemistry.* 2000, **39**: 11205-11215.
24. Parniak, M.A. and Sluis-Cremer, N., Inhibitors of HIV-1 reverse transcriptase. *Adv. Pharmacol.* 2000, **49**: 67-109.
25. Poznanski, J., Bretner, M., Kulikowski, T., Balzarini, J., Van Aerschot, A. and De Clercq, E., Synthesis, solution conformation and anti-HIV activity of novel 3'-substituted-2',3'-dideoxy-5-hydroxymethyluridines and their 4,5-substituted analogues. *Antivir. Chem. Chemother.* 2003, **14**: 127-138.
26. Reddy, D.V., Jagannadh, B. and Kunwar, A.C., NMR study of dideoxynucleotides with anti-human immunodeficiency virus (HIV) activity. *J. Biochem. Biophys. Methods.* 1996, **31**: 113-121.
27. Rodriguez, J.B., Marquez, V.E., Nicklaus, M.C., Mitsuya, H. and Barchi, J.J., Jr., Conformationally locked nucleoside analogues. Synthesis of dideoxycarbocyclic nucleoside analogues structurally related to neplanocin C. *J. Med. Chem.* 1994, **37**: 3389-3399.
28. Russ, P.L., Gonzalez-Moa, M.J., Vu, B.C., Sigano, D.M., Kelley, J.A., Lai, C.C., Deschamps, J.R., Hughes, S.H. and Marquez, V.E., North- and south-bicyclo[3.1.0]hexene nucleosides: the effect of ring planarity on anti-HIV activity. *ChemMedChem.* 2009, **4**: 1354-1363.
29. Schinazi, R.F., Hernandez-Santiago, B.I. and Hurwitz, S.J., Pharmacology of current and promising nucleosides for the treatment of human immunodeficiency viruses. *Antiviral Res.* 2006, **71**: 322-334.
30. Siddiqui, M.A., Driscoll, J.S., Marquez, V.E., Roth, J.S., Shirasaka, T., Mitsuya, H., Barchi, J.J., Jr. and Kelley, J.A., Chemistry and anti-HIV properties of 2'-fluoro-2',3'-dideoxyarabinofuranosylpyrimidines. *J. Med. Chem.* 1992, **35**: 2195-2201.
31. Siddiqui, M.A., Hughes, S.H., Boyer, P.L., Mitsuya, H., Van, Q.N., George, C., Sarafinanos, S.G. and Marquez, V.E., A 4'-C-ethynyl-2',3'-dideoxynucleoside analogue highlights the role of the 3'-OH in anti-HIV active 4'-C-ethynyl-2'-deoxy nucleosides. *J. Med. Chem.* 2004, **47**: 5041-5048.
32. Sluis-Cremer, N. and Tachedjian, G., Mechanisms of inhibition of HIV replication by non-nucleoside reverse transcriptase inhibitors. *Virus Res.* 2008, **134**: 147-156.
33. Stewart, J.J.P., Optimization of parameters for semiempirical methods I. Method. *J. Comput. Chem.* 1989, **10**: 209-220.
34. *SYBYL 7.3*, Tripos International: 1699 South Hanley Rd., St. Louis, Missouri, 63144, USA.
35. Tuske, S., Sarafianos, S.G., Clark, A.D., Jr., Ding, J., Naeger, L.K., White, K.L., Miller, M.D., Gibbs, C.S., Boyer, P.L., Clark, P., Wang, G., Gaffney, B.L., Jones, R.A., Jerina, D.M., Hughes, S.H. and Arnold, E., Structures of HIV-1 RT-DNA complexes before and after incorporation of the anti-AIDS drug tenofovir. *Nat. Struct. Mol. Biol.* 2004, **11**: 469-474.
36. Van Wijk, J., Huckriede, B.D., Ippel, J.H. and Altona, C., Furanose sugar conformations in DNA from NMR coupling constants. *Methods Enzymol.* 1992, **211**: 286-306.
37. Westhof, E., Plach, H., Cuno, I. and Ludemann, H.-D., Proton magnetic resonance studies of 2'-, 3'-, and 5'-deoxyadenosine conformations in solution. *Nucelic Acids Res.* 1977, 4: 939-953.
38. White, K.L., Chen, J.M., Feng, J.Y., Margot, N.A., Ly, J.K., Ray, A.S., Macarthur, H.L., McDermott, M.J., Swaminathan, S. and Miller, M.D., The K65R reverse transcriptase mutation in HIV-1 reverses the excision phenotype of zidovudine resistance mutations. *Antivir. Ther.* 2006, **11**: 155-163.

Nucleic Acids Research, 2012, Vol. 40, No. 1 **345–359**
doi:10.1093/nar/gkr694

Biochemical, inhibition and inhibitor resistance studies of xenotropic murine leukemia virus-related virus reverse transcriptase

Tanyaradzwa P. Ndongwe[1], Adeyemi O. Adedeji[1], Eleftherios Michailidis[1], Yee Tsuey Ong[1], Atsuko Hachiya[1], Bruno Marchand[1], Emily M. Ryan[1], Devendra K. Rai[1], Karen A. Kirby[1], Angela S. Whatley[1], Donald H. Burke[1,2], Marc Johnson[1], Shilei Ding[3], Yi-Min Zheng[1], Shan-Lu Liu[1,3], Ei-Ichi Kodama[4], Krista A. Delviks-Frankenberry[5], Vinay K. Pathak[5], Hiroaki Mitsuya[6], Michael A. Parniak[7], Kamalendra Singh[1] and Stefan G. Sarafianos[1,2,*]

[1]Christopher Bond Life Sciences Center, Department of Molecular Microbiology & Immunology, University of Missouri, School of Medicine, Columbia, [2]Department of Biochemistry, University of Missouri, Columbia, MO 65211, USA, [3]Department of Microbiology and Immunology, McGill University, Montreal, QC, Canada, [4]Department of Internal Medicine, Division of Emerging Infectious Diseases, Tohoku University School of Medicine, Sendai, Japan, [5]HIV Drug Resistance Program, National Cancer Institute-Frederick, Frederick MD, [6]Department of Internal Medicine, Kumamoto University School of Medicine, Kumamoto Japan & Experimental Retrovirology Section, HIV/AIDS Malignancy Branch, NIH, Bethesda MD and [7]Department of Molecular Genetics & Biochemistry, University of Pittsburgh School of Medicine, Pittsburgh, PA, USA

Received June 3, 2011; Revised August 5, 2011; Accepted August 8, 2011

ABSTRACT

We report key mechanistic differences between the reverse transcriptases (RT) of human immunodeficiency virus type-1 (HIV-1) and of xenotropic murine leukemia virus-related virus (XMRV), a gammaretrovirus that can infect human cells. Steady and pre-steady state kinetics demonstrated that XMRV RT is significantly less efficient in DNA synthesis and in unblocking chain-terminated primers. Surface plasmon resonance experiments showed that the gammaretroviral enzyme has a remarkably higher dissociation rate (k_{off}) from DNA, which also results in lower processivity than HIV-1 RT. Transient kinetics of mismatch incorporation revealed that XMRV RT has higher fidelity than HIV-1 RT. We identified RNA aptamers that potently inhibit XMRV, but not HIV-1 RT. XMRV RT is highly susceptible to some nucleoside RT inhibitors, including Translocation Deficient RT inhibitors, but not to non-nucleoside RT inhibitors. We demonstrated that XMRV RT mutants K103R and Q190M, which are equivalent to HIV-1 mutants that are resistant to tenofovir (K65R) and AZT (Q151M), are also resistant to the respective drugs, suggesting that XMRV can acquire resistance to these compounds through the decreased incorporation mechanism reported in HIV-1.

INTRODUCTION

Xenotropic murine leukemia virus-related virus (XMRV) is a gammaretrovirus that was first identified in some prostate cancer tissues (1,2) While some subsequent reports confirmed the presence of XMRV in prostate cancer samples (3–6), several others found little or no evidence of the virus in patient samples (7–9). XMRV DNA was also reported in 67% of patients with chronic fatigue syndrome (CFS) (10), but several subsequent studies in Europe and the USA failed to identify XMRV DNA in CFS patients or healthy controls (11–15). Hence, the relevance of XMRV to human disease remains unclear (16) and have been challenged (17). Most recently, it has been reported that XMRV has been generated through recombination of two separate proviruses suggesting that the association of XMRV with human disease is due to contamination of human samples with virus originating from this recombination event (18). Nonetheless, as a retrovirus that can infect human cells, XMRV can be very helpful in advancing our understanding of the mechanisms of retroviral reverse transcription, inhibition and drug resistance.

---

*To whom correspondence should be addressed. Tel: +1 573 882 4338; Fax: +1 573 884 9676; Email: sarafianoss@missouri.edu

XMRV RT is similar to the Moloney murine leukemia virus (MoMLV) RT, which has been the subject of structural and biochemical studies (19–24). Most of the differences between these gammaretroviral enzymes are at the RNase H domain (Supplementary Figure S1). Comparisons of human immunodeficiency virus type-1 (HIV) RT with MoMLV RT have revealed structural and sequence differences (21). For example, HIV-1 RT is a heterodimer composed of two related subunits (25,26) [reviewed in (27,28)]. Its larger p66 subunit (~66 kDa) contains both the polymerase and RNase H domains; the smaller p51 subunit, (~51 kDa), is derived from the p66 subunit by proteolytic cleavage and its role is to provide structural support and optimize RT's biochemical functions (29). In contrast, structural studies have demonstrated that MoMLV RT is a monomer of about 74 kDa, although one study reported that it may form a homodimer during DNA synthesis (30). So far, there are no published biochemical or structural studies on XMRV RT. Hence, the present study on this enzyme and its comparison to related enzymes provides an excellent opportunity to advance our biochemical understanding of the mechanism of reverse transcription, its inhibition and drug resistance.

MATERIALS AND METHODS

Expression and purification of XMRV, HIV-1 and MoMLV RTs

The plasmid pBSK-XMRV containing the coding sequence of XMRV RT from the VP62 clone (GenBank: DQ399707.1) was chemically synthesized and optimized for bacterial expression by Epoch Biolabs Inc (Missouri City, Texas, USA). The 2013 bp XMRV RT sequence was amplified from pBSK-XMRVRT by PCR, using the forward and reverse primers 1 (all primer sequences are shown in Supplementary Table S1), resulting in NdeI and HindIII restriction sites. Drug resistant XMRV RT mutants Q190M and K103R (equivalent to HIV-1 Q151M RT and K65R) were generated by site-directed mutagenesis using forward and reverse primers 2 and 3. The digested amplicons were ligated into pET-28a (Novagen), resulting into a construct that expresses an N-terminal hexahistidine tag. pET-28a-MRT encoding full-length wild-type MoMLV RT was provided by Dr M. Modak (New Jersey Medical School, Newark NJ, USA).

Expression and purification of MoMLV and XMRV RTs were carried out similarly to our previously published protocols (23,24). Briefly, RTs were expressed in BL21-pLysS *Escherichia coli* (Invitrogen) grown at 37°C and induced with 150 µM IPTG at OD_{600} 0.8, followed by 16 h growth at 17°C. A cell pellet from a 3 l culture was incubated with 40 ml lysis buffer (50 mM Tris–HCl, pH 7.8, 500 mM NaCl, 1 mM PMSF, 0.1% NP-40, 1% sucrose and 2 mg/ml lysozyme), then sonicated and centrifuged at 15,000 g for 30 min. The supernatant was diluted 2-fold in Buffer A (50 mM Tri–HCl pH 7.8, 1 mM PMSF, 4% streptomycin sulfate and 10% sucrose), stirred on ice for 30 min and centrifuged. The supernatant was loaded on a Ni-NTA column and bound proteins were washed with 20 ml Buffer B (20 mM Tris–HCl pH 7.5, 500 mM NaCl) and 5 mM imidazole, followed by 20 ml Buffer B with 75 mM imidazole. RT was eluted in 2 ml fractions with 20 ml buffer B containing 300 mM imidazole. Fractions with RT were pooled and further purified by size exclusion chromatography (Superdex 75; GE Healthcare). RTs (>95% pure) were stored in 50 mM Tris–HCl pH 7.0, 100 mM NaCl, 1 mM DTT, 0.1% NP-40 and 30% glycerol in 10 µl aliquots at −20°C. Protein concentrations were determined by measuring UV_{280} (molar extinction coefficients of 106 and 103 $M^{-1} cm^{-1}$ for XMRV and MoMLV RT).

HIV-1 RT was cloned in a pETduo vector and purified as described previously (29,31,32). Oligonucleotide sequences (IDT-Coralville, IA, USA) of DNA/RNA substrates are shown in Supplementary Table S1. Nucleotides were purchased from Fermentas (Glen Burnie, MD, USA). They were treated with inorganic pyrophosphatase (Roche Diagnostics, Mannheim, Germany) as described previously (33) to remove PPi that might interfere with excision assays.

Steady state kinetics

Steady state parameters K_m and k_{cat} for dATP incorporation were determined using single nucleotide incorporation gel-based assays. XMRV RT and MoMLV RT reactions were carried out in 50 mM Tris–HCl pH 7.8, 60 mM KCl, 0.1 mM DTT, 0.01% NP-40 and 0.01% bovine serum albumin (BSA) (Reaction Buffer) with 6 mM $MgCl_2$ or 1.5 mM $MnCl_2$, 0.5 mM EDTA, 200 nM or 100 nM T_{d26}/5′-Cy3-P_{d18b}, 20 nM or 5 nM RT for XMRV and MoMLV RTs, respectively and varying concentrations of dNTP in a final volume of 10 µl. The reactions for HIV-1 RT were carried out in Reaction Buffer with 100 nM T_{d26}/5′-Cy3-P_{d18b}, 10 nM HIV-1 RT and 6 mM $MgCl_2$ in a 20 µl reaction. All the concentrations mentioned here and in subsequent assays reflect final concentration of reactants otherwise mentioned reactions were stopped after 15 min for XMRV, 4 min for MoMLV RT, and 2.5 min for HIV-1. The products were resolved on 15% polyacrylamide–7M urea gels. The gels were scanned with a Fuji Fla-5000 PhosphorImager (Stamford, CT, USA) and the bands were quantified using MultiGauge. Results were plotted using GraphPad Prism 4. K_m and k_{cat} were determined graphically using Michaelis–Menten equation.

Gel mobility shift assays

Formation of RT-DNA binary complex: 20 nM T_{d31}/5′-Cy3-P_{d18a} (Supplementary Table S1) was incubated for 10 minutes with increasing amounts of MoMLV or XMRV RT in 50 mM Tris–HCl pH 7.8, 0.01% BSA, 5 mM $MgCl_2$ and 10% (v/v) sucrose. The complexes were resolved on native 6% polyacrylamide 50 mM Tris–borate gel and visualized as described above.

Active site titration and determination of $K_{D.DNA}$

Active site concentrations and kinetic constants of DNA binding for XMRV, HIV-1 and MoMLV RTs were determined using pre-steady state experiments. Reactions with XMRV and MoMLV RTs were carried out in the reaction buffers listed above. For XMRV RT 100 nM protein was pre-incubated with increasing concentrations of $T_{d31}/5'$-Cy3-P_{d18a}, followed by rapid mixing with a reaction mixture containing 5 mM $MgCl_2$ and 100 µM next incoming nucleotide (dATP). The reactions were quenched at various times (5 ms to 4 s) by adding EDTA to a final concentration of 50 mM. The amounts of 19-mer product were quantified and plotted against time. The data were fit to the following burst equation:

$$P = A(1 - e^{-k_{obs}t}) + k_{ss}t \qquad (1)$$

where A is the amplitude of the burst phase that represents the RT–DNA complex at the start of the reaction, k_{obs} is the observed burst rate constant for dNTP incorporation, k_{ss} is the steady state rate constant and t is the reaction time. The rate constant of the linear phase (k_{cat}) was estimated by dividing the slope of the linear phase by the enzyme concentration. The active site concentration and T/P binding affinity ($K_{D.DNA}$) were determined by plotting the amplitude (A) against the concentration of T/P. Data were fit to the quadratic equation (Equation 2) using non-linear regression:

$$A = 0.5(K_D + [RT] + [DNA] - \sqrt{0.25(K_D + [RT] + [DNA])^2 - ([RT] + [DNA])} \qquad (2)$$

where K_D is the dissociation constant for the RT–DNA complex, and [RT] is the concentration of active polymerase. HIV-1 RT's DNA binding affinity was determined as previously described (29).

Surface plasmon resonance assay

We used surface plasmon resonance (SPR) to measure the binding constants of XMRV and HIV-1 RTs to double-stranded DNA. Experiments were carried out using a Biacore T100 (GE Healthcare). To prepare the sensor chip surface we used the 5′-biotin-T_{d37}/P_{d25} oligonucleotide (Supplementary Table S1). One hundred and twenty RUs of this DNA duplex were bound in channel 2 of a streptavidin-coated sensor chip [Series S Sensor Chip SA (certified)] by flowing a solution of 0.1 µM DNA at a flow rate of 10 µl/min in a buffer containing 50 mM Tris pH 7.8, 50 mM NaCl. The binding constants were determined as follows: RT binding was observed by flowing solutions containing increasing concentrations of the enzyme (0.2, 0.5, 1, 2, 5, 10, 20, 50, 100 and 200 nM) in 50 mM Tris pH 7.8, 60 mM KCl, 1 mM DTT, 0.01% NP40 and 10 mM $MgCl_2$ in channels 1 (background) and 2 (test sample) at 30 µl/min. The trace obtained in channel 1 was subtracted from the trace in channel 2 to obtain the binding signal of RT. This signal was analyzed using the Biacore T100 Evaluation software to determine $K_{D.DNA}$, k_{on} and k_{off}.

Pre-steady state kinetics of dNTP incorporation

The optimal nucleotide incorporation rates (k_{pol}) were obtained by pre-steady state kinetics analysis using single nucleotide incorporation assays. A solution containing XMRV RT (150 nM final concentration) and $T_{d31}/5'$-Cy3-P_{d18a} (40 nM) was rapidly mixed with a solution of $MgCl_2$ (5 mM) and varying dATP (5–200 µM) for 0.1 to 6 s before quenching with EDTA (50 mM) (all concentrations in parentheses are final, unless otherwise stated). Products were resolved and quantified as described above. Burst phase incorporation rates and substrate affinities were obtained from fitting the data to Equation 1. Turnover rates (k_{pol}), dNTP binding to the RT-DNA complex ($K_{d.dATP}$), and observed burst rates (k_{obs}) were fit to the hyperbolic equation:

$$k_{obs} = (k_{pol}[dNTP])/(K_{d.dNTP} + [dNTP]) \qquad (3)$$

HIV-1 RT's DNA binding affinity was determined as previously described (29).

Fidelity of DNA synthesis

The fidelity (error-proneness) of XMRV RT was determined and compared with that of MoMLV RT and HIV-1 RT by primer extension assays using 10 nM heteropolymeric $T_{d100}/5'$-Cy3-P_{d18a}. Reactions (10 µl) were carried out in Reaction Buffer containing all four dNTPs (100 µM each) or only three dNTPs (missing either dATP, dGTP or dTTP) at 100 µM each. Incubations of the XMRV and MoMLV (50 nM) reactions were at 37°C for 45 min and 30 min for HIV-1 RT (20 nM). Reactions were initiated by adding dNTPs, stopped with equal volume of formamide-bromophenol blue, and an aliquot was run on a 16% polyacrylamide–7M urea gel.

Kinetics of mismatch incorporation

For these experiments, instead of including the next correct nucleotide (dATP) in the polymerase reactions, we used dTTP as the mismatched incoming nucleotide. Hence, 50 nM XMRV RT was pre-incubated with 35 nM $T_{d31}/5'$-Cy3-P_{d18a} in reaction mixture. Reactions were initiated by adding dTTP (5–750 µM) and 5 mM $MgCl_2$, followed by incubation (37°C) for 5 min, due to the decreased mismatch incorporation rate of XMRV. For MoMLV RT, 30 nM RT and 20 nM DNA used and the reactions were carried out for 2.5 minutes. For HIV-1, 30 nM RT, 20 nM DNA and 0–200 µM nucleotide were used and the reactions were carried out for 2.5 min. The amount of extended primer was quantified and plotted against the concentration of dTTP. The data were used to derive the $K_{d.dNTP}$ of incorrect nucleotide binding, the rate k_{pol} (using Equations 1 and 3) and the efficiency of the misincorporation reaction ($k_{pol}/K_{d.dTTP}$).

Determination of *in vivo* fidelity

ANGIE P cells, which contain a retroviral vector (GA-1) that encodes a bacterial β-galactosidase gene (*lacZ*) and a neomycin phosphotransferase gene, were plated (5×10^6 cells/100 mm dish) and after 24 h were transfected using the calcium phosphate precipitation method with a plasmid expressing either XMRV or amphotropic MLV (AM-MLV) (three independent transfections per vector). After 48 h, the culture medium with XMRV or (AM-MLV) was harvested, serially diluted and used to infect

D17 target cells (2×10^5 cells/60 mm dish) in the presence of polybrene. The infected D17 cells were selected for resistance to G418 (400 µg/ml) in the presence of 1 µM AZT to suppress reinfection, and characterized by staining with 5-bromo-4-chloro-3-indoyl-β-D-galacto-pyranoside (X-Gal) ~2 weeks after G418 selection. The frequencies of inactivating mutations in *lacZ* quantified as described before (blue versus white colonies) (34).

Processivity of DNA synthesis—trap assay

Processivity reactions were carried out in Reaction Buffer containing 20 nM T_{d100}/P_{d18}, 100 µM of each dNTP, 30 nM HIV-1 RT, 50 nM MoMLV RT or 100 nM XMRV RT and 1µg/µl unlabeled calf thymus DNA trap in 50 µL. Enzymes were pre-incubated with T_{d100}/P_{d18} for 1 min before adding dNTPs (100 µM each) together with the calf thymus DNA trap. Reactions were incubated at 37°C, and 10 µl aliquots were taken out at 3, 7.5 and 15 min for HIV-1 RT or at 7.5, 15 and 30 min for XMRV RT and MoMLV RT, and mixed with equal volume of loading dye. The effectiveness of the trap was determined by pre-incubating the enzyme with the trap before adding T_{d100}/P_{d18}. Control DNA synthesis was measured in absence of trap under the same conditions. Reaction products were resolved as above.

Single turnover processivity assays

Thirty nanomolar T_{d31}/5′-Cy3-P_{d18a} was pre-incubated for 10 min with 100 nM XMRV or 50 nM MoMLV RT in Reaction Buffer, then rapidly mixed with 100 µM dNTPs, 5 mM $MgCl_2$ for varying times (0.1–45 s) before quenching with EDTA (50 mM final). Single turnover processivity of HIV-1 RT was assayed with 40 nM enzyme, 20 nM DNA and 50 µM of each nucleotide were used. The reaction products were resolved and quantified as described above. The data were fit to a one-phase exponential decay equation for the elongation of the 18-mer primer. The rates of appearance and extension of products from subsequent nucleotide incorporations (19- and 27-mer) were obtained by fitting the intensities of corresponding bands to double exponential (Equation 4):

$$P = A(1 - e^{-k_1 t}) + (e^{-k_2 t}) + C \qquad (4)$$

where A is the amplitude, P is the amount of 19-mer, 20-mer or higher length products, k_1 is the rate of product generation, k_2 the rate of subsequent elongation and C a constant (29,35).

Assays for reverse transcriptase inhibition

DNA synthesis by 50 nM XMRV RT or MoMLV RT was carried out in Reaction Buffer using 20 nM T_{d100}/5′-Cy3-P_{d18a}, 2.5 µM dNTP, 5 mM $MgCl_2$ and varying amounts of NRTI (0–100 µM). Reactions were quenched with 95% formamide after 1 h incubation at 37°C (38). In experiments with aptamers 10 nM XMRV RT, 20 nM T_{d31}/5′-Cy3-P_{d18a} and 50 µM dNTPs were used in the presence of varying amounts of aptamer for 30 min (0–500 nM for m.1.3; 0–25 nM for m.1.4 and m.1.1FL). The inhibition of DNA polymerization was monitored by resolving the products on 15% polyacrylamide–7 M urea gels and visualized as described above. Bands corresponding to full extension products were quantified using MultiGauge Software and IC_{50}s were obtained from dose–response curves using GraphPad Prism.

PPi- and ATP-dependent excision and rescue of $T/P_{AZT\text{-}MP}$ or $T/P_{EFdA\text{-}MP}$

The ability of enzymes to use PPi or ATP to unblock template-primers that had AZT-MP ($T/P_{AZT\text{-}MP}$) or EFdA-MP ($T/P_{EFdA\text{-}MP}$) at their 3′ primer ends was measured as follows: 20 nM of $T/P_{AZT\text{-}MP}$ or $T/P_{EFdA\text{-}MP}$ were prepared as described before (32). They were incubated at 37°C with either 60 nM HIV-1 RT or 200 nM XMRV RT in the presence of 0.15 mM PPi or 3.5 mM ATP for PPi- or ATP-dependent rescue reactions, respectively. Reactions were initiated by the addition of $MgCl_2$ (6 mM). Aliquots were removed at different times (0–90 min) and analyzed as above. Rescue assays were performed in the presence of 100 µM dATP to prevent EFdA-MP reincorporation, 0.5 µM dTTP, 10 µM ddGTP and 10 mM $MgCl_2$.

Molecular modeling

The sequence of XMRV RT from the VP62 clone was aligned with that of MoMLV RT (PDB: 1RW3) (21,22) using ClustalW. To generate the homology model of XMRV RT, we used the Prime protocol of the Schrödinger software suite (Schrödinger Inc. NY). The resulting molecular model was further energy minimized by OPLS2005 force field using the Impact option of Schrödinger. The final model was validated with PROCHECK v.3.5.4.

RESULTS

Comparison of RT sequences

The XMRV and MoMLV enzymes are closely related (~95% sequence identity) with most of the differences between them being in the RNase H domain (Supplementary Figure S1). While XMRV and MoMLV differ significantly from HIV-1 RT, the known polymerase motifs (A–F) are well conserved in all three enzymes (Supplementary Figure S1). Specifically, the active site aspartates in Motifs A and C (Figure 9) (D150, D224, D225 in XMRV RT; D150, D224, D225 in MoMLV RT; D110, D185, D186 in HIV-1 RT) are conserved in all three RTs. Also, the three enzymes are similar in Motif B, which is involved in dNTP binding and multidrug resistance (AZT and dideoxy-nucleoside drugs) through the decreased incorporation mechanism (27,39–41). Specifically, all three enzymes have a glutamine at the start of this motif (Q151 in HIV-1 RT, Q190 in XMRV RT and Q190 in MoMLV RT). Motif D includes HIV-1 RT residues L210 and T215, which when mutated they enhance excision of AZT from the AZT-terminated primer terminus. This motif is mostly different in XMRV and MoMLV RTs, where the corresponding residues are N226 and A231 (Supplementary Figure S1). K219 of HIV-1 RT Motif D is proximal to the dNTP-binding pocket and is also conserved in the other enzymes (K235). The DNA primer grip (Motif E) (36,42) in HIV-1 RT ($M_{230}G_{231}Y_{232}$) is slightly different in the gammaretroviral enzymes ($L_{245}G_{246}Y_{247}$). Motif F at the fingers subdomain of all enzymes has two conserved lysines that bind the triphosphate of the dNTP (K65 and K72 in HIV-1 RT; K103 and K110 in XMRV and MoMLV RTs).

Several HIV-1 residues involved in NRTI resistance have the resistance mutations in XMRV and MoMLV RTs (Table 1). Hence, XMRV and MoMLV RTs have a Val as the X residue (codon 223) of the conserved YXDD sequence of Motif C. An M184V mutation at this position in HIV-1 RT causes strong, steric hindrance-based, resistance to 3TC and FTC (43–45), and to a lesser extent to ddI, ABC [reviewed in (46)], and translocation defective RT inhibitors (TDRTIs) (43) (Table 1). Similarly, the M41L mutation, which causes excision-based AZT resistance in HIV is already present in XMRV and MoMLV RT (L81, Table 1). The gammaretroviral enzymes differ from HIV-1 RT in several other HIV drug resistance sites (HIV residues 62, 67, 69, 70, 75, 77, 115, 210, 215) (Table 1). Finally, there are also differences in residues that are essential for NNRTI binding in HIV-1 RT: W229 changes to Y268 in XMRV RT, Y181 to L220, Y188 to L227 and G190 to A229 (Table 1) (27,28,47–49).

Preparation of MoMLV and XMRV RTs

The sequence coding for full-length XMRV RT from the VP-62 clone (NCBI RefSeq: NC_007815) (1) was optimized for expression in bacteria, synthesized by Epoch Biolabs and cloned as described in 'Materials and Methods' section. Both XMRV RT and MoMLV RT were tagged with a hexahistidine sequence at the N-terminus and expressed with a yield of ~2 mg/l of culture. Purified enzymes (>95% pure, Supplementary Figure S2) were stored at −20°C. The presence of NP-40 or glycerol was critical for enzyme stability.

Steady state kinetics of nucleotide incorporation

Initial polymerase activity assays using $T_{d31}/5'\text{-Cy3-}P_{d18a}$ displayed overall slower polymerase activity of XMRV RT compared to HIV-1 and MoMLV RTs. This observation led us to investigate the steady state nucleotide incorporation properties of XMRV RT using single nucleotide incorporation assays. The estimated values for k_{cat} ($19.9\,\text{min}^{-1}$ for HIV-1 RT (32), $3.3\,\text{min}^{-1}$ for MoMLV RT, $0.6\,\text{min}^{-1}$ for XMRV RT) and $K_{m.dNTP}$ (0.07 µM for HIV-1 RT (32), 3.3 µM for MoMLV RT, 3.0 µM for XMRV RT) show that XMRV RT has a drastically reduced efficacy ($k_{cat}/K_{m.dNTP}$) at nucleotide incorporation, compared to both MoMLV and HIV-1 RTs.

DNA binding affinity

To assess if the efficiency of XMRV RT was also affected by a lower DNA binding affinity we measured the DNA binding affinity of the enzymes using three methods: gel-mobility shift assays, pre-steady state kinetics and SPR. Gel-mobility shift assays showed that the $K_{D.DNA}$ for XMRV RT was marginally higher than that for HIV-1 RT and MoMLV RT (data not shown) (50) suggesting weaker binding to DNA.

DNA binding affinity using pre-steady state kinetics

Pre-steady state kinetics allows estimation of the fraction of active polymerase sites as well as the $K_{D.DNA}$ value for the enzyme. The amplitudes of DNA extensions using XMRV RT and/or MoMLV RT at varying DNA concentrations were plotted against the DNA concentration and

Table 1. HIV-1 RT drug resistance mutations with wild-type XMRV RT and MoMLV RT residues

	HIV-1 residue numbers	HIV-1 RT wt	HIV-1 resistance mutations					XMRV RT wt	MoMLV RT wt
			3TC	ABC	TDF	D4T	EFdA		
Thymidine analog mutations (TAMs)	184	M	V	V	–	–	V	V223	V223
	41	M	–	L	L	L	–	L81	L81
	67	D	–	N	N	N	–	G105	G105
	210	L	–	W	W	W	–	N226	N226
	215	T	–	FY	FY	FY	–	A231	A231
	219	K	–			QE	–	K235	K235
Non-thymidine analog regimen mutations	65	K	RN	RN	RN	RN	–	K103	K103
	70	K	EG	EG	EG	–	–	D108	D108
	74	L	–	VI	–	–	–	V112	V112
	75	V	–	TM	M	TM	–	Q113	Q113
	115	Y	–	F	F		–	F155	F155
	69	T	Ins	Ins	Ins	Ins	–	N107	N107
Multi-NRTI resistance mutations	151	Q	M	M	M	M	–	Q190	Q190
	62	A	V	V	V	V	–	P104	P104
	75	V	–	I	–	I	–	Q113	Q113
	77	F	–	L	–	L	–	L115	L115
	116	F	–	Y	–	Y	–	F156	F156
TDRTI Mutations	184	M	V	V	–	–	V	V223	V223
	165	T	–	–	–	–	R	H204	H204

The HIV-1 RT data are based on data from the Stanford HIV Database (85).
wt = wild-type.

the data were fit to the quadratic equation (Equation 2), yielding a $K_{D.DNA}$ of 33 nM for XMRV RT, 19 nM for MoMLV RT (Table 2) and 12.5 nM for HIV-1 RT (32). These values did not change significantly when tested with DNA of different lengths (data not shown). Hence, the transient kinetic experiments confirmed the findings of the gel-mobility shift assays showing XMRV RT to have lower DNA binding affinity than HIV-1 RT.

Binding kinetics of XMRV and HIV-1 RT to double-stranded DNA

Measurements of $K_{D.DNA}$ using gel-mobility shift assays and pre-steady state kinetic methods do not offer insights regarding the kinetics of binding and release of nucleic acid from the viral polymerases. Hence, we used SPR to measure directly DNA binding and the DNA dissociation components of the $K_{D.DNA}$. We attached on the SPR chip a nucleic acid biotinylated at the 5′ template end and immobilized it on a streptavidin sensor chip. Various concentrations of either XMRV or HIV-1 RT were flowed over the chip to measure the association (k_{on}) and dissociation (k_{off}) rates of the enzymes in real time (Figure 1). HIV-1 RT had considerably slower dissociation rates than XMRV RT, and longer dissociation phases were needed to obtain reliable values.

Several methods were tested to best fit our data. The 'heterogeneous ligand' method gave the best fit for both XMRV and HIV-1 RT. In this model the x^2 values for DNA binding to XMRV and HIV-1 RT were 9.3 RU^2 and 48.1 RU^2, respectively, compared to 15.1 RU^2 and 152 RU^2 when we tried fitting the data in a 'homogeneous ligand' model. The former model assumes that RT binds DNA in two different modes and provides two association (k_{on}) and two dissociation constants (k_{off}).

Our data show that XMRV RT has a slightly faster rate of association (k_{on}) than HIV-1 RT. We measured two k_{on} values of $7.3 \times 10^6 M^{-1}s^{-1}$ and $8.2 \times 10^4 M^{-1}s^{-1}$ for XMRV RT versus $7.6 \times 10^5 M^{-1}s^{-1}$ and $1.2 \times 10^6 M^{-1}s^{-1}$ for HIV-1 RT. Interestingly, the dissociation rate of XMRV RT was significantly faster than that of HIV-1 RT (0.28 s^{-1} and 0.0045 s^{-1} for XMRV RT and 7.8×10^{-4} $s^{-1}$and 0.0076 s^{-1} for HIV-1 RT) (Table 3). This difference in dissociation rate resulted in a $K_{D.DNA}$ at least 1 order of magnitude higher for XMRV RT compared to HIV-1 RT (38 and 54 nM versus 1.0 and 6.1 nM for XMRV and HIV-1 RT, respectively) (Table 3).

Table 2. Kinetic parameters of DNA binding and synthesis by HIV-1 and XMRV RTs

Nucleotide affinity and incorporation	HIV-1 RT[a]	MoMLV RT	XMRV RT
$K_{d.dNTP}$ (μM)	1.3 ± 0.4	25 ± 5.3	26.6 ± 6.5
k_{pol} (s^{-1})	24.4 ± 0.9	14.1 ± 0.8	8.9 ± 0.6
$k_{pol}/K_{d.dNTP}$ ($s^{-1} \cdot \mu M^{-1}$)	18.8	0.56	0.33
DNA binding affinity:			
$K_{D.DNA}$ (nM)	12.5	19.0	32.5

[a] HIV-1 RT data published previously (29).

Nucleotide binding affinity and optimal incorporation efficiency

A transient-state kinetics approach was used to estimate the dNTP binding affinity ($K_{d.dNTP}$) and maximum nucleotide incorporation rate (k_{pol}) (55). The rates at varying concentrations of next incoming nucleotide (dATP) were determined by plotting the amount of extended primer as a function of time. The rates were then plotted against dATP concentration. The data were fit to a hyperbola (Equation 3). The $K_{d.dNTP}$ for XMRV RT is 26.6 μM and the k_{pol} is 8.9 s^{-1} (Figure 2) (Table 2). Under similar conditions the $K_{d.dNTP}$ and k_{pol} were 1.3 μM and 24.4 s^{-1} for HIV-1 RT (29) and 25 μM and 14.1 s^{-1} for MoMLV RT.

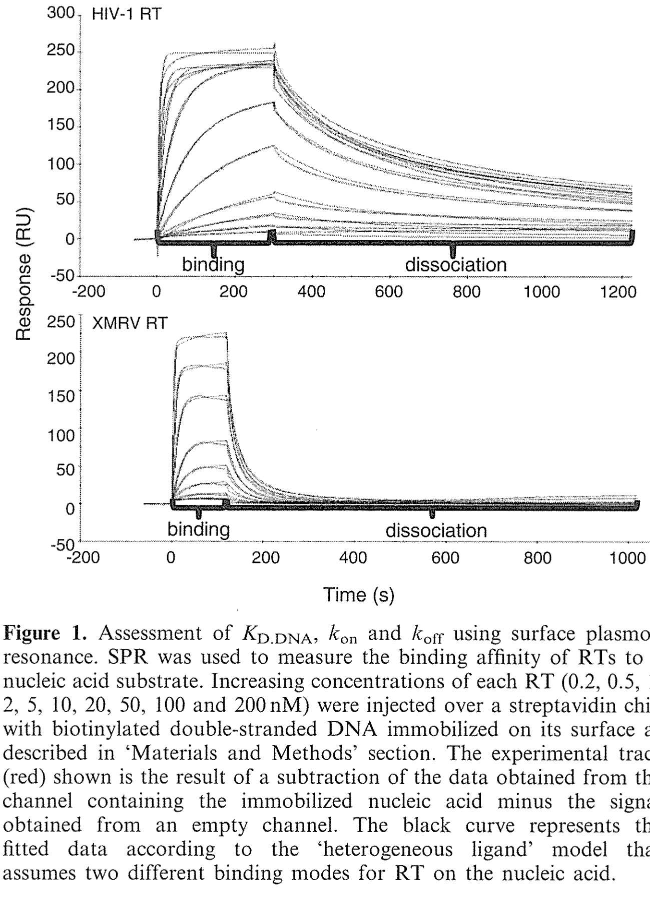

Figure 1. Assessment of $K_{D.DNA}$, k_{on} and k_{off} using surface plasmon resonance. SPR was used to measure the binding affinity of RTs to a nucleic acid substrate. Increasing concentrations of each RT (0.2, 0.5, 1, 2, 5, 10, 20, 50, 100 and 200 nM) were injected over a streptavidin chip with biotinylated double-stranded DNA immobilized on its surface as described in 'Materials and Methods' section. The experimental trace (red) shown is the result of a subtraction of the data obtained from the channel containing the immobilized nucleic acid minus the signal obtained from an empty channel. The black curve represents the fitted data according to the 'heterogeneous ligand' model that assumes two different binding modes for RT on the nucleic acid.

Table 3. DNA binding constants for HIV-1 and XMRV RTs from surface plasmon resonance

	HIV-1 RT	XMRV RT
k_{on} ($M^{-1}.s^{-1}$)	7.6×10^5	7.3×10^6
k_{off} (s^{-1})	7.8×10^{-4}	2.8×10^{-1}
$K_{D.DNA1}$ (nM)	1	38 (38-fold)[a]
k_{on} ($M^{-1}.s^{-1}$)	1.2×10^6	8.2×10^4
k_{off} (s^{-1})	7.6×10^{-3}	4.5×10^{-3}
$K_{D.DNA2}$ (nM)	6.1	54 (9-fold)[a]

[a] Increase in $K_{D.DNA}$ (decrease in affinity) with respect to HIV-1 RT. ($K_{D1\text{-}XMRV\ RT}/K_{D1HIV\text{-}1\text{-}RT}$ and $K_{D2\text{-}XMRV\ RT}/K_{D2HIV\text{-}1\text{-}RT}$).

Fidelity of nucleotide incorporation

To assess whether XMRV RT displays high nucleotide incorporation fidelity we monitored the incorporation of three dNTPs by XMRV RT and compared with HIV-1 RT (52). The results of fidelity assay are shown in Figure 3. The lanes marked '4dNTPs' for all enzymes represent the DNA synthesis using a T_{d100}/5′-Cy3-P_{d18a} template-primer in the presence of all four dNTPs. The subsequent lanes, marked '-dNTP', correspond to the synthesis of DNA in the absence of that specific deoxynucleotide triphosphate. The comparison of the DNA synthesis in the absence of one nucleotide by HIV-1 RT, MoMLV RT and XMRV RT shows that HIV-1 and MoMLV RTs were able to misincorporate and extend the primer beyond the missing nucleotide more efficiently than XMRV RT, suggesting that the latter is a less error prone DNA polymerase. It should be noted that the higher fidelity of XMRV is not the result of measuring a smaller number of errors because of the decreased replication rate, as the assay conditions were optimized to allow production of the same amount of full length product in the presence of all four dNTPs for and MoMLV RTs. To further investigate the fidelity of DNA synthesis by XMRV RT, the kinetics of mismatch nucleotide incorporation were carried out in a quantitative manner by monitoring the incorporation of single mismatched nucleotide under pre-steady state conditions. The estimated $K_{D.dTTP}$ (mismatch) and k_{pol} values show that XMRV RT has a lower affinity for a mismatched nucleotide but comparable turnover number than MoMLV RT, suggesting that the observed higher fidelity over MoMLV RT is due to differences during the nucleotide-binding step (Table 4). However, compared to HIV-1 RT, XMRV RT has decreased both affinity and incorporation rate, suggesting that its higher fidelity is the result of both decreased binding of mismatched nucleotides and slow rate of incorporation.

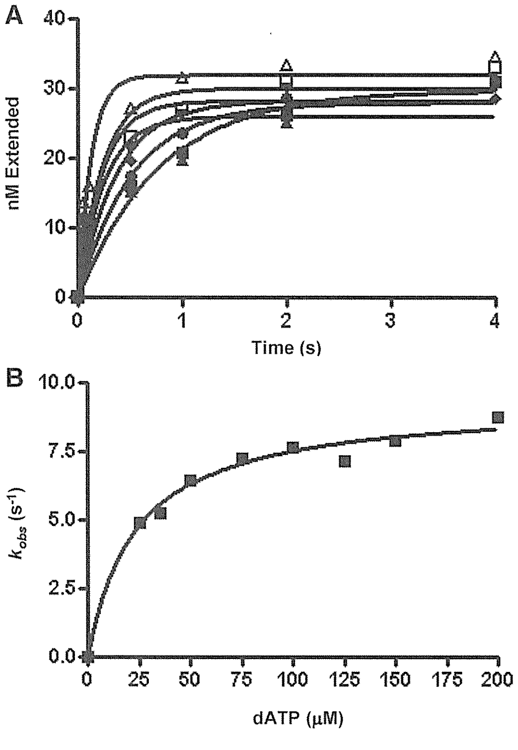

Figure 2. Pre-steady state kinetics of nucleotide incorporation by XMRV RT. 150 nM XMRV RT was pre-incubated with 40 nM T_{d31}/5′-Cy3-P_{d18a} rapidly mixed with a solution containing $MgCl_2$ (5 mM) and varying concentrations of dATP: 25 μM (filled square), 35 μM (filled triangle), 50 μM (filled inverted triangle), 75 μM (filled rhombus), 100 μM (filled circle), 125 μM (open square) and 150 μM (open triangle); and incubated for 0.1 to 6 s before being quenched with EDTA. The DNA product for each dATP concentration was fit to the burst equation (**A**). The burst amplitudes generated for each dATP concentration were then fit to a hyperbola equation (**B**) yielding the optimal rates of dNTP incorporation; k_{pol} (8.9 s^{-1}) and dNTP binding to the RT-DNA complex; $K_{d.dATP}$ (26.6 μM).

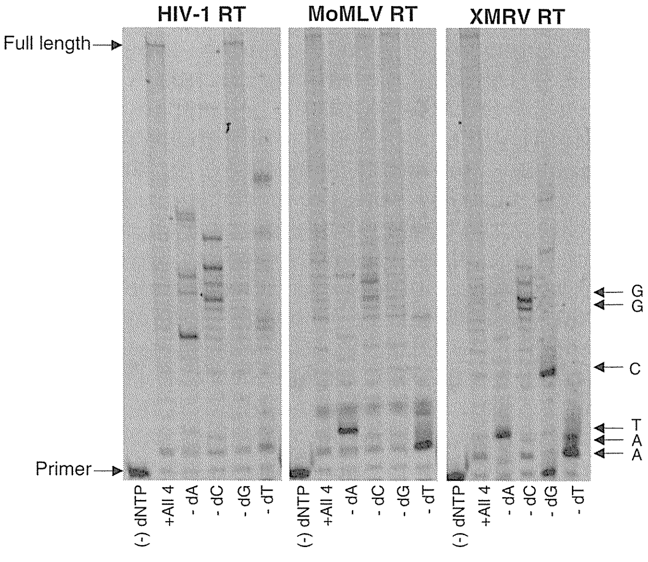

Figure 3. Comparison of *in vitro* fidelity of HIV-1, MoMLV and XMRV RTs. Extension of 10 nM T_{d100}/5′-Cy3-P_{d18a} by HIV-1 RT, MoMLV RT or XMRV RT (20, 50 and 50 nM, respectively) in the presence of 150 μM each of three out of four nucleotides (the missing nucleotide is marked at the bottom of each lane). Reactions were run for 30 min for HIV-1 RT and 45 min for XMRV RT and MoMLV RT. For each enzyme the first lane in each set shows the position of unextended primer, the second lane shows full extension in the presence of all four dNTPs, and each consecutive lane shows extension in the presence of three dNTPs. The arrows on the right mark the expected pauses based on the indicated composition of the template strand.

Table 4. Kinetics of mismatch incorporation for HIV-1, MoMLV and XMRV RTs

Enzyme	HIV-1 RT	MoMLV RT	XMRV RT
$K_{d.dNTP}$ (μM)	9 ± 0.3	38.9 ± 11.6	256 ± 72
k_{pol} (s^{-1})	6.81 ± 1.2	0.16 ± 0.01	0.15 ± 0.018
$k_{pol}/K_{d.dNTP}$ (s^{-1}•μM)	0.756	0.0041	0.00058
Fidelity[a]	0.04	0.007	0.002

[a] Fidelity is the ratio of the incorporation efficiency ($k_{pol}/K_{d.dNTP}$) of the mismatched nucleotide (dTTP) over that of the correct (dATP) ([k_{pol}/K_d]dTTP/[k_{pol}/K_d]dATP).

Intracellular fidelity by measuring LacZ mutation frequency

The ANGIE P cells used for this assay are a D17-based encapsidating cell line and contain an MLV-based retroviral vector (GA-1), which encodes a bacterial β-galactosidase gene (*lacZ*) and a neomycin phosphotransferase gene (*neo*). Replication fidelity is a measure of the frequency of *lacZ* inactivation and was determined by measuring *lacZ* non-expressing white colonies. The results show that the number of white colonies was not statistically different in the case of XMRV as compared to AM-MLV, suggesting that under these conditions the fidelity of XMRV is not significantly different than that of AM-MLV (Figure 4).

Processivity of DNA synthesis

Processivity is the probability of translocation of a polymerase along a template and predicts the number of cycles of nucleotide incorporation during one productive enzyme–DNA binding event. We assessed XMRV RT's processivity of DNA synthesis in comparison to HIV and MoMLV RTs using both a gel-based trap assay and a quantitative pre-steady state assay. In the gel-based assay, the enzymes were pre-incubated with template-primer, then the reaction was initiated by the addition of all four nucleotides together with calf thymus DNA, which was used as a trap to bind free enzyme dissociated from the substrate during the course of the reaction (38). The length of the DNA product is an inverse measure of termination probability, as previously described. As a control, we used lanes where no trap was present; establishing that the same amount of total polymerase activity (processive and non-processive) is provided in all cases. The results indicate that XMRV RT is less processive than HIV-1 and MoMLV RTs with shorter DNA product after 30 min of reaction in the presence of trap (Figure 5).

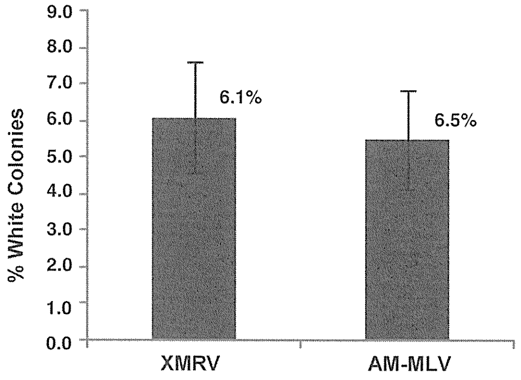

Figure 4. Comparison of *in vivo* fidelity of XMRV with amphotropic MLV. The ANGIE P cells used for this assay contain a retroviral vector (GA-1), which encodes a bacterial β-galactosidase gene (*lacZ*) and a neomycin phosphotransferase gene. Replication fidelity is measured by the frequency of *lacZ* inactivation resulting in an increase in white colonies. The fidelity differences between the two viruses are not statistically significant (error bars represent standard error from three independent experiments).

To measure processivity quantitatively we applied a single turnover processivity assay developed by Patel *et al.* (35) (Figure 6). In this assay, the rates of consecutive nucleotide incorporations under single turnover conditions are monitored. The rate of elongation incorporation (k_1) and the rate of processive DNA synthesis (k_2) (Equation 4) were calculated at several template positions for each enzyme. The ratio of the rate of processive DNA synthesis to the rate of nucleotide incorporation (k_2/k_1) is referred to as the processivity index (35). The absolute values of these constants for HIV-1 RT, XMRV and MoMLV RT and their ratios are collected in Table 5. XMRV RT is clearly the least processive for each extension product. The difference in processivity varies significantly depending on sequence or sequence context (decrease in processivity from 3-fold up to 10-fold). While the current data do not allow generalization of rules for pausing at specific sites, this clearly shows consistently that XMRV is not as efficient as MoMLV RT in polymerizing processively through 'difficult spots'.

Susceptibility of XMRV RT to NRTIs, TDRTIs and NNRTIs

Previous studies have shown that XMRV is inhibited by some antivirals (53–56). However, the susceptibility of XMRV RT has not been tested against a wide variety of

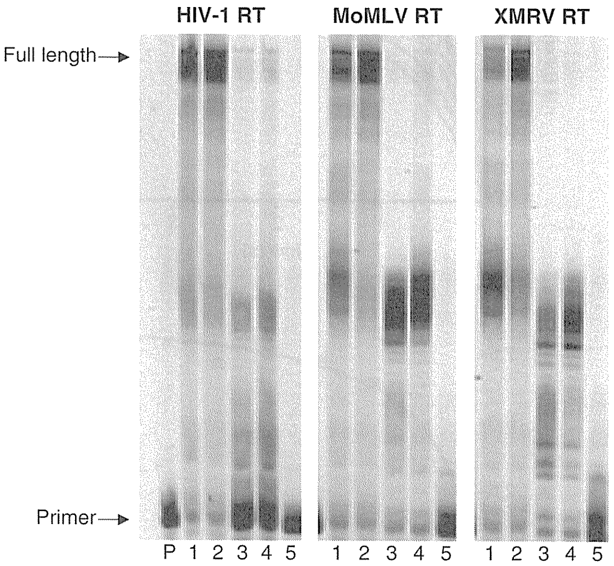

Figure 5. Processivity (trap assay) of HIV-RT, MoMLV RT and XMRV RT. DNA synthesis was monitored in the presence of calf thymus DNA as an enzyme trap. Each enzyme (30 nM HIV RT, 100 nM MoMLV RT or 100 nM XMRV RT) was pre-incubated with 40 nM T_{d100}/Cy3-P_{d18a}. Lanes 1 and 2 of each set show unlimited DNA synthesis in the absence of trap for 5 and 10 min for HIV-1 RT and 10 and 40 min for XMRV RT and MoMLV RT. In Lanes 3 and 4 the reaction is initiated by the addition of dNTPs (100 µM each) together with the calf thymus DNA trap (0.5 µg/µl) such that the products generated represent a single processive synthesis event for the respective time points for each enzyme. Lane 5 shows the effectiveness of the trap determined by incubating the calf thymus DNA with the enzyme before addition of labeled template-primer. Processive primer extension by HIV-1 RT and MoMLV RT in Lanes 4–6 of the left and middle panel is higher than by XMRV RT in Lanes 4–6 of the right panel.

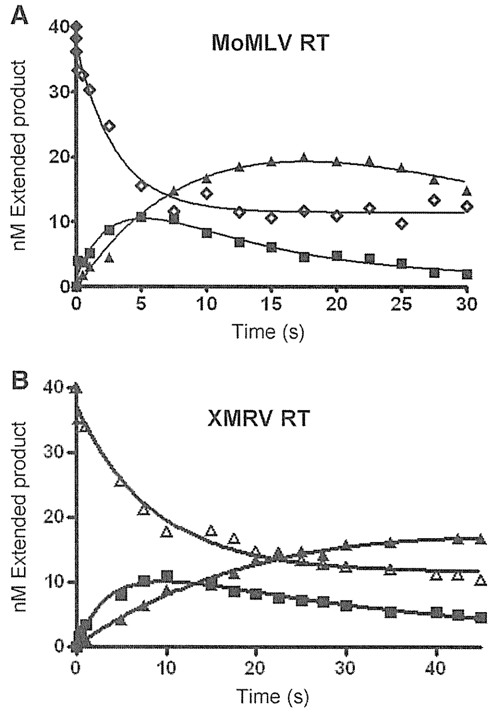

Figure 6. Single-turnover processivity assays. 30 nM T_{d31}/Cy3-P_{d18a} was combined with 100 nM XMRV RT or 50 nM MoMLV RT in RT buffer before rapidly mixing with all four dNTPs (100 µM each) and 5 mM $MgCl_2$ for varying incubation times (0.05–45 s) and quenching with EDTA. Extension of the 18-mer primer (open rhombus) ((open triangle) for XMRV RT) into 19-mer (filled square) and 22-mer (filled square), by MoMLV RT (**A**) and XMRV RT (**B**) was fit to a double exponential equation to determine rates of product appearance, and subsequent processive extension of those products (rates shown in Table 5).

Table 5. Single turnover processivity parameters of HIV-1, MoMLV and XMRV RTs

Template site	Processivity index (k_2/k_1)		
	HIV-1 RT	MoMLV RT	XMRV RT
1	6.98	0.31	0.12

```
                        1
3′-CAT TGA CAA GCT CGT GGT TAC GAT CGA TAC C
5′-Cy3-GTA ACT GTT CGA GCA CCT
```

The template site position monitored is underlined and labeled.

nucleoside RT inhibitors (NRTIs) that block replication by chain-terminating the primer, or by preventing translocation after their incorporation into the nascent DNA chain (TDRTIs) (32,57,58). In addition, the susceptibility of XMRV RT to non-nucleoside RT inhibitors (NNRTIs) or RNA aptamers that can be selected to block reverse transcriptases (59–63) has not been established.

Hence, we performed gel-based primer extension assays in the presence of various inhibitors. As shown in Table 6, most of the HIV-1 RT inhibitors also block XMRV RT with significantly varying IC_{50}s. The most potent inhibitors tested were ENdA (4′-ethynyl-2-amino-2′-deoxyadenosine) followed by EFdA. EFdA was also potent at inhibiting wild-type XMRV replication in cell culture with an EC_{50} of 40 nM from three independent experiments (standard error was 10 nM).

Table 6. Inhibition of XMRV and MoMLV RTs

Compound	IC_{50} (µM)	
	XMRV RT	MoMLV RT
Adefovir-DP	0.92	1.02
Tenofovir-DP	6.4	1.51
D4T-TP	0.77	2.37
3TC-TP	21	10
EFdA-TP	0.43	0.29
ENdA-TP	0.14	0.18

D4T, stavudine or 2′,3′-dehydro-2′,3′-deoxythymidine; 3TC, lamivudine; EFdA, 4′-ethynyl-2-fluoro-2′-deoxyadenosine; ENdA, 4′-ethynyl-2-amino-2′-deoxyadenosine.

Unlike HIV-1 RT, XMRV RT and MoMLV RT lack the two tyrosine residues (Y181 andY188 in HIV-1 RT) (Supplementary Figure S1) that are known to contribute to NNRTI binding. Hence, the gammaretroviral enzymes were not inhibited by the NNRTIs tested (TMC-125 and efavirenz) (Supplementary Figure S3).

Susceptibility of XMRV RT to RNA aptamers

We also tested XMRV RT's susceptibility to three independent RNA aptamers that had been previously selected against MoMLV RT (60). The aptamers inhibited XMRV RT to varying extents with IC_{50}s ranging from 2 to 52 nM (Figure 7). Most notable was the m.1.1FL aptamer which gave IC_{50}s of 2 and 4 nM for XMRV RT (Figure 7) and MoMLV RT respectively, without inhibiting HIV-1 RT (data not shown). These inhibition assays utilized truncated forms of aptamers m.1.3 and m.1.4 lacking the original primer-binding segments of the aptamers, demonstrating that these 5′ and 3′ segments are not required.

PPi-mediated excision activity of XMRV RT

A key mechanism of NRTI resistance in HIV-1 RT is based on inhibitor excision from the primer end, using a pyrophospholytic reaction (64,65). The pyrophosphate donor *in vivo* is likely to be ATP, although PPi can efficiently unblock NRTI-terminated primers. This excision activity is present in wild-type HIV-1 RT, and is enhanced in the presence of AZT-resistance mutations. We measured the ability of wild-type XMRV to unblock primers terminated with AZT or EFdA in the presence of PPi. We found that unlike HIV-1 RT that excised AZT-MP efficiently under these conditions, XMRV RT had considerably lower excision activity (Figure 8). Similar excision experiments where ATP was used instead of PPi showed that XMRV is very inefficient in ATP-based excision as compared to HIV-1 RT (data not shown).

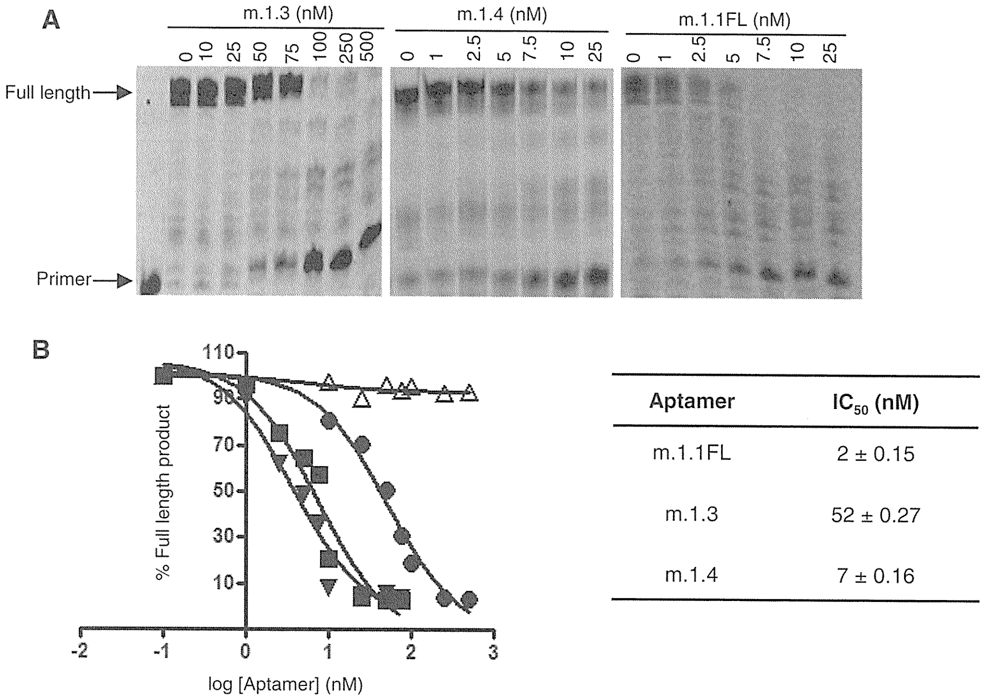

Aptamer	IC_{50} (nM)
m.1.1FL	2 ± 0.15
m.1.3	52 ± 0.27
m.1.4	7 ± 0.16

Figure 7. Inhibition of XMRV RT by RNA aptamers. 10 nM XMRV RT was incubated with increasing amounts of RNA aptamer in Reaction Buffer for 5 min at 37°C followed by addition of 20 nM T_{d31}/Cy3-P_{d18a} and 50 µM of each dNTP. (**A**) The reactions were stopped after 30 min and resolved on a polyacrylamide gel. The predicted secondary structures of each aptamer were generated by mfold. (**B**) The percent full extension was quantified for m.1.1FL (filled inverted triangle), m.1.3 (filled circle) and m.1.4 (filled square) and data points fit to one-site competition non-linear regression using GraphPad Prism 4 to calculate IC_{50}. HIV-1 RT was not susceptible to m.1.1FL (open triangle). (Errors represent data deviation from the fit).

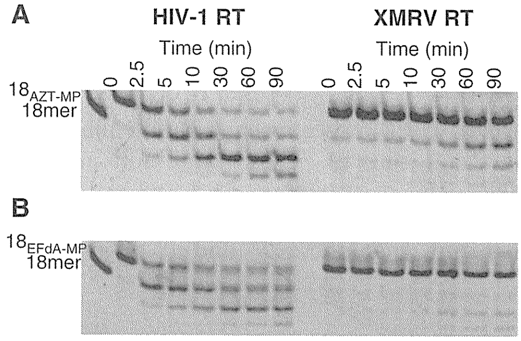

Figure 8. PPi-mediated unblocking of AZT-(A) and EFdA-(B) terminated DNA. About 20 nM of (**A**) AZT- or (**B**) EFdA-terminated T_{d31}/Cy3-P_{d18c} (T/P_{AZT-MP} or $T/P_{EFdA-MP}$) was incubated with HIV-1 RT (60 nM) or XMRV RT (200 nM) in the presence of 150 µM PPi and 6 mM $MgCl_2$. Aliquots of the reactions were stopped at different time points (0–90 min) and resolved on a 15% polyacrylamide–7M urea gel as described in the 'Materials and Methods' section.

Susceptibility of mutant XMRV RTs to AZT-TP and tenofovir-DP

The HIV-1 RT mutation Q151M confers resistance to AZT by enhancing discrimination of the nucleotide analog leading to its reduced incorporation (37,66–68). Another HIV-1 RT mutation, K65R, decreases susceptibility to tenofovir (69,70). Since AZT and tenofovir are potent inhibitors of XMRV (Table 6) (54–56), we wanted to investigate whether the XMRV RT mutant equivalents of HIV Q151M and K65R (XMRV Q190M and K103R) would confer XMRV RT resistance to AZT and tenofovir. We constructed these mutant clones and tested their susceptibility to AZT and tenofovir in the same manner as wild-type XMRV RT. Interestingly, Q190M XMRV RT has a decreased susceptibility to AZT (approximately 5-fold increase in the IC_{50}). Similarly, the K103R XMRV RT mutant enzyme was less susceptible to tenofovir, increasing the IC_{50} by at least 2-fold.

Molecular model of XMRV RT

Given the significant sequence similarity between XMRV and MoMLV RTs, the resulting homology model of XMRV RT is highly similar to MoMLV RT (>1.5Å rms) and of excellent quality. Since the input structure of MoMLV RT did not contain the RNase H domain of the enzyme, the XMRV RT model is also missing this domain. The molecular model of the polymerase domain of XMRV RT is shown in Figure 9. An alignment of the MoMLV RT crystal structure (22) with the XMRV RT homology model highlights the few changes in the polymerase domain of XMRV RT. These are L29 (P in MoMLV), Q234 (L in MoMLV), R238 (Q in MoMLV) and N422 (D in MoMLV). From these, residue 422 is located in the nucleic acid binding cleft and may contribute to differences in the interactions with nucleic acid substrate. However, most of the differences between the gammaretroviral enzymes are in their RNase H domains and also in the first 30 N-terminal residues of the polymerase domain, for which we do not have structural

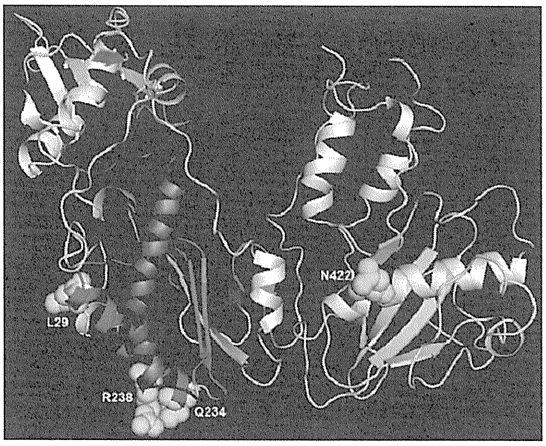

Figure 9. Molecular model of XMRV RT. Ribbons diagram of XMRV RT with the conserved polymerase Motifs color-coded: Motif A (green), B (brown), C (purple), D (red), E (orange) and F (blue). The residues that differ from MoMLV's polymerase domain are shown in ball and stick representation.

information since they were not included in the original crystal structure of MoMLV RT. The differences between XMRV RT and HIV-1 RT are very significant. Unlike the HIV enzyme, XMRV RT appears to be a monomer in solution. Moreover, alignment of the HIV-1 RT–DNA complex with XMRV RT based on their active sites at the palm subdomains shows that the thumb subdomain of XMRV RT would have to be repositioned to be able to accommodate nucleic acid.

DISCUSSION

Early studies reported the presence of XMRV in stromal cells from prostate cancer patient samples and also in CFS clinical samples. Some of the subsequent studies confirmed these findings whereas several others failed to identify XMRV in prostate cancer or in CFS patients, even when same samples were used (71). It was recently reported that human sample contamination with mouse DNA can occur frequently (17,72–74). Moreover, two coauthors from this study have recently demonstrated that XMRV is the product of recombination events between two MLV proviruses, suggesting that XMRV may not be relevant to human disease (18). Nonetheless, XMRV is still an important human retrovirus and comparisons with HIV can provide valuable insights into the fundamental mechanisms of DNA polymerization, RT inhibition and drug resistance. (75).

There is high degree of sequence similarity between the XMRV and MoMLV RTs (95% amino acid identity), and much less so with HIV-1 RT. Based on gel filtration experiments we conclude that unlike HIV-1 RT, but similar to MoMLV RT, XMRV RT exists in solution primarily as a monomer. We also included comparisons with HIV-1 RT in this study as it has been extensively studied and provides an excellent frame of reference.

We report here that there are significant differences in the DNA polymerization efficiency of the three enzymes. Although the polymerase active sites of the XMRV and MoMLV enzymes are almost identical, there is a considerable decrease in the efficiency of nucleotide incorporation by XMRV RT. Most differences in sequence are at the RNase H domain and are likely to affect polymerization by changing the positioning of DNA at the polymerase active site.

We have recently solved the crystal structure of the XMRV RNase H at high resolution (1.5Å) (pdb 3P1G) (Kirby, K.A. *et al.*, submitted for publication). We observed major differences in affinity for nucleic acid that we determined with gel-mobility shift assays and with pre-steady state kinetics. SPR experiments dissected in more detail the specific defect of XMRV RT in binding DNA. Surprisingly, XMRV RT can associate very rapidly with DNA, even more so than HIV-1 RT (Figure 1 and Table 3). However, it dissociates from DNA much faster than the HIV enzyme, resulting in an overall reduced binding affinity. A possible reason for the fast association and dissociation rates of XMRV RT may be the apparent monomeric state, which might offer facile access to the nucleic acid binding cleft, although with less contacts and lower affinity than HIV-1 RT, which is a heterodimer (76,77). This high rate of XMRV RT dissociation from DNA likely contributes to the decreased processivity observed in our study, and may have consequences in the recombination rates of this virus.

Previous sequences of XMRV from prostate cancer tumors showed low variability, suggesting that the virus may have a high fidelity of replication (1,10). Our study demonstrated that HIV-1 RT and MoMLV RT incorporated mismatched nucleotides and extended past the mismatches more efficiently than XMRV RT. Pre-steady state kinetics established that the higher overall fidelity of XMRV RT over MoMLV RT is due to a lower affinity for mismatched nucleotides. When compared to HIV-1 RT, however, XMRV RT has differs in both the nucleotide binding and incorporation steps. Nonetheless, XMRV did not have higher fidelity than a related amphotropic MLV virus or HIV-1 in a cell-based assay. It is possible that the high dNTP concentration in dividing cells can suppress mismatching events. We have previously shown (39) that as nucleotide concentrations vary in different cell lines, this can affect viral susceptibility to NRTIs, and possibly in this case also incorporation of mismatched nucleotides. Additional cell-based studies using multiple cell lines and a large panel of viruses should provide a better understanding of the relation between *in vivo* and *in vitro* fidelity.

Early studies have reported susceptibility of XMRV to some antiretrovirals that have been used in the treatment of HIV infection (53–56). In those studies the compounds were tested at the virus level. To better understand the interactions of inhibitors at their RT target level we tested here the ability of these and several more compounds to block the polymerase activity of XMRV RT. We found that two TDRTIs, EFdA-TP and ENdA-TP were very potent RT inhibitors (IC_{50}s: 0.43 μM and 0.14 μM, respectively). Unlike other NRTIs, these compounds have a 3′ OH group and are known to efficiently inhibit HIV replication by blocking translocation (32,58,78).

Preliminary experiments demonstrated that they also block XMRV RT by the same mechanism (data not shown).

In HIV, moderate resistance to EFdA is conferred by the emergence of the M184V mutation at the conserved X position of the conserved YXDD motif of the polymerase active site. Interestingly, XMRV and MoMLV RTs already have a valine (V223) at this position. This difference is likely to contribute to the better potency of EFdA against HIV-1 RT than XMRV RT or MoMLV RT (57,58). It may also contribute to the decreased ability of XMRV RT to unblock chain-terminated primers, as was also reported for M184V HIV-1 RT (79) and to the enhanced fidelity reported here for XMRV RT, which is also reminiscent of the previously reported high fidelity of M184V HIV-1 RT (80,81). Nonetheless, despite the presence of a Val in the YMDD motif of XMRV RT we found EFdA to inhibit very efficiently replication-competent or pseudotyped XMRV, with submicromolar EC$_{50}$s (40 and 110 nM, respectively).

Previously, highly potent aptamers were selected to inhibit MoMLV RT (60). We demonstrate here that the three aptamers we tested have varying potency against XMRV RT. Aptamer m.1.1FL was the most potent inhibitor of XMRV RT and MoMLV RT in *in vitro* assays (IC$_{50}$ = 2 and 4 nM, respectively). The fact that XMRV and MoMLV RTs are inhibited by the same aptamers at comparable efficiencies suggests that the RT residues that are different in the two enzymes are not critical to the binding of the aptamer. In contrast, heterodimeric HIV-1 RT has a very different binding cleft and is not inhibited by these aptamers.

Tenofovir is an essential component of HIV therapies and is also a potent inhibitor of XMRV RT. HIV resistance to tenofovir is conferred by a single codon mutation (K65R). HIV-1 RT residue 65 is known to interact with the incoming dNTP or the activated tenofovir analog (tenofovir diphosphate) (82). K65R causes resistance to tenofovir by lowering the k_{pol} for the incorporation of the inhibitor into the nascent DNA. We prepared XMRV RT with the equivalent mutation, K103R, and determined that it has decreased susceptibility to tenofovir. Hence, it is possible for XMRV to develop tenofovir resistance through the same mechanism as HIV-1 RT. HIV resistance to AZT can occur by either decreased binding/incorporation or increased excision of the chain-terminating NRTI (33,83). HIV-1 RTs containing the M41L, D67N, K70R, T215Y/F, K219E/Q mutations show enhanced removal of AZT. Our experiments show that unlike wild-type HIV-1 RT, XMRV RT is not able to excise NRTI-terminated primers. Similarly, it was previously shown that MoMLV RT is not capable of unblocking chain-terminated primers (33).

In HIV, decreased binding of AZT is conferred initially in the presence of the primary Q151M mutation, followed by secondary mutations F77L, A62V, V75I and F116Y (27,47,84). XMRV RT already differs from wild-type HIV-1 RT in the first three of these residues (P104, Q113 and L115 versus A62, V75 and F77) (Table 1). We demonstrated that introducing the primary Q→M mutation at the equivalent XMRV RT site (Q190M) resulted in an enzyme with decreased susceptibility to AZT. Hence, it appears that these residues can confer AZT resistance to XMRV by reduced incorporation of nucleotide analogs, as is the case in HIV-2 (41). At this point we do not know if introduction of as yet unknown mutations could endow XMRV RT with the ability to unblock chain-terminated nucleic acids. The details of the molecular mechanism of XMRV resistance to tenofovir and AZT are under investigation.

In conclusion, our study provides detailed biochemical analysis of the mechanisms of polymerization, inhibition, fidelity, processivity and drug resistance of XMRV RT and how it compares with the closely related enzyme MoMLV RT and the more distantly related HIV-1 RT. The findings enhance our understanding of the basic mechanisms of reverse transcription.

SUPPLEMENTARY DATA

Supplementary Data are available at NAR Online.

ACKNOWLEDGEMENTS

The content of this publication does not necessarily reflect the views or policies of the Department of Health Human Services, nor does mention of trade names, commercial products or organizations imply endorsement by the U.S. Government.

FUNDING

NIH grants (AI076119, AI079801, and AI094715, to S.G.S.), (AI074389, to D.H.B.), (AI079801 to M.A.P.); NIH Bench-to-Bedside Award and the Intramural Research Program of the NIH, National Cancer Institute, Center for Cancer Research (to V.K.P); Ministry of Knowledge and Economy, Bilateral International Collaborative R&D Program, Republic of Korea; Canadian Institutes of Health Research (CIHR) and University of Missouri (to S-L.L.); amfAR Mathilde Krim Fellowship and a CIHR Fellowship (to B.M.). Funding for open access charge: NIH grants (AI076119, AI094715, AI074389, AI079801).

Conflict of interest statement. None declared.

REFERENCES

1. Urisman,A., Molinaro,R.J., Fischer,N., Plummer,S.J., Casey,G., Klein,E.A., Malathi,K., Magi-Galluzzi,C., Tubbs,R.R., Ganem,D. *et al.* (2006) Identification of a novel gammaretrovirus in prostate tumors of patients homozygous for R462Q RNASEL variant. *PLoS Pathog.*, **2**, e25.
2. Malathi,K., Dong,B., Gale,M. Jr. and Silverman,R.H. (2007) Small self-RNA generated by RNase L amplifies antiviral innate immunity. *Nature*, **448**, 816–819.
3. Arnold,R.S., Makarova,N.V., Osunkoya,A.O., Suppiah,S., Scott,T.A., Johnson,N.A., Bhosle,S.M., Liotta,D., Hunter,E., Marshall,F.F. *et al.* XMRV infection in patients with prostate cancer: novel serologic assay and correlation with PCR and FISH. *Urology*, **75**, 755–761.
4. Dong,B., Kim,S., Hong,S., Das Gupta,J., Malathi,K., Klein,E.A., Ganem,D., Derisi,J.L., Chow,S.A. and Silverman,R.H. (2007) An